Organic sulfur from source to sink in low-sulfate Lake Superior

[1,2]Alexandra A. Phillips*, [1]Imanol Ulloa, [2]Emily Hyde, [2]Julia Agnich, [1]Lewis Sharpnack, [1]Katherine G. O'Malley, [3]Samuel M. Webb, [2,4]Kathryn M. Schreiner, [2,5]Cody S. Sheik, [2,6]Sergei Katsev, [1]Morgan Reed Raven

[1]*Department of Earth Science, University of California Santa Barbara, Santa Barbara, CA, USA*
[2]*Large Lakes Observatory, University of Minnesota Duluth, Duluth, MN, USA*
[3]*Stanford Synchrotron Radiation Lightsource, Stanford University, Menlo Park, CA, USA*
[4]*Department of Chemistry & Biochemistry, University of Minnesota Duluth, Duluth, MN, USA*
[5]*Department of Biology, University of Minnesota Duluth, Duluth, MN, USA*
[6]*Department of Physics and Astronomy, University of Minnesota Duluth, Duluth, MN, USA*

**Corresponding author:* phillips.alexandra.a@gmail.com

Target Journal: Limnology and Oceanography

Keywords
(5-12)
sulfur cycle, carbon cycle, Lake Superior, sulfurization, lipid sulfurization, sulfate reduction, organic sulfur, pyrite, pyritization, microbial community, sulfate reducers, low-sulfate

Author Contributions
AAP, KMS, CSS, SK, and MRR designed the study. AAP, EH, KMS, CSS, and SK collected the samples. KMS, CSS, SK, and MRR secured research funding. All authors contributed to data collection and analysis. AAP and KGO created the figures. AAP wrote the paper with input from all authors.

Abstract

(250 words)

Organic sulfur plays a crucial role in the biogeochemistry of aquatic sediments, especially in low sulfate (<500 μM) environments like freshwater lakes and the Archean Ocean. To better understand organic sulfur cycling in these systems, we followed organic sulfur in Lake Superior sediments from source to sink. We identified microbial populations with shotgun metagenomic sequencing and characterized geochemical species in porewater and solid phases. In anoxic sediments, we found an active sulfur cycle fueled by oxidized organic sulfur at the depth interface between dissolved oxygen and abundant iron. Sediment incubations indicated a microbial capacity to hydrolyze sulfonates, sulfate esters, and sulfonic acids to sulfate. Gene abundances for dissimilatory sulfate reduction (*dsrAB*) increased with depth and coincided with sulfide maxima. Eight metagenome assembled genomes (MAGs) contained *dsrAB* genes, including canonical families from the orders of Desulfobaccales, Thermodesulfovibrionales, and Syntrophales. Despite these indicators of sulfide formation, dissolved sulfide concentrations at this site are low (< 40 nM) due to efficient and simultaneous sinks, including both pyritization and organic matter sulfurization. Immediately below the oxycline, pyrite accounted for 13% of total sedimentary sulfur, and its distribution with depth may be linked to historical positions of the oxycline. Both free and intact lipids also accumulated disulfides in this same interval near the oxycline, reflecting rapid sulfurization. Our investigation revealed a new model of sulfur cycling in a low-sulfate environment that likely extends to other modern lakes and possibly the ancient ocean, with organic sulfur both fueling sulfate reduction and reacting with the resultant sulfide.

Introduction

While sulfur cycling evolved in low-sulfate (μM) environments during the Archean (Crowe et al. 2014; Mateos et al. 2022), our knowledge of ancient sulfur metabolisms and reactions is largely rooted in studies of high-sulfate systems like the modern ocean (28 mM; Jørgensen et al. 2019). The sulfur cycles in high- and low-sulfate systems, however, are fundamentally different in their constraints. The sulfur budget in the modern ocean is dominated by a massive reservoir of seawater sulfate that is six orders of magnitude greater than the largest pool of organic sulfur (Ksionzek et al. 2016; Moran and Durham 2019). In low-sulfate systems like lakes organic sulfur is much more significant to sulfur budgets, for example, acting as an alternative fuel for sulfur reduction via hydrolysis (Fakhraee et al. 2017; Fakhraee and Katsev 2019). Sulfides produced in these low-sulfate systems may experience different sinks than marine sulfides, with cascading impacts on metal cycling, biomarker preservation, and organic carbon remineralization (de Leeuw and Sinninghe-Damste 1990; Saito et al. 2003). Currently, we know little about the pathways, mechanisms, and dominant species driving organic sulfur cycling in low-sulfate aquatic sediments – or how these interact with the biogeochemical cycles of carbon and iron. We turn to a useful proxy environment to address these gaps: oligotrophic, low-sulfate (<40 μM), high-iron (30–80 μM) Lake Superior.

Initial characterizations of Lake Superior sediments revealed enigmatic sulfate profiles with sub-surface maxima (Fakhraee et al. 2017). Unlike the modern ocean, where sulfate is typically highest at the sediment interface due to diffusion from the water column (Zhu et al. 2021), Lake Superior appears to experience a significant efflux of sulfate from the sediments to the water column. Fakhraee et al. (2017) hypothesized that microbial sulfate reduction, supported via hydrolysis of organic sulfur, was supplying this excess sedimentary sulfate. Reaction-transport models suggested that up to 50% of Lake Superior sulfate reduction could be supported via this mechanism. We aim to provide new constraints on Lake Superior's organic sulfur cycle. Namely, confirmation and identification of key sulfate reducers in the microbial community, the oxidation state of organic sulfur that hydrolyzes to sulfate, and the ultimate sinks of resultant sulfide in the environment. These insights will improve our understanding of sulfur cycling in modern low-sulfate environments and bridge knowledge to past environments like the Archean Ocean.

Prior investigations of Lake Superior's microbial community have largely focused on photosynthesis in the water column (Fahnenstiel et al. 1986; Ivanikova et al. 2007; Reed and Hicks 2011; Sheik et al. 2022), reflecting the importance of this freshwater resource for drinking, recreation, and hydroelectric power (O'Beirne et al. 2017). Sedimentary studies have thus far focused on specialized cycles like those of metals (Dittrich et al. 2015; Palermo and Dittrich 2016) and nitrogen (Small et al. 2016; Crowe et al. 2017). One study even deemed sulfate reduction in Lake Superior sediments as an "insignificant process" (Carlton et al. 1989). Despite later research suggesting otherwise, including modeled sulfide accumulation (Fakhraee et al. 2017), no studies have surveyed the microbial community for sulfur cycling microorganisms. Notably, despite low predicted sulfide, Lake Superior sediments were recently found to contain abundant sulfide oxidizers like *Thioploca*, suggesting active cryptic cycling (McKay et al. 2023).

Sources of organic sulfur to Lake Superior sediments primarily reflect phytoplankton sources from the water column with some terrestrial input (Zigah et al. 2011; Li et al. 2012). The organic sulfur composition of phytoplankton biomass is poorly constrained but includes a range of sulfur

oxidation states in proteins, carbohydrates, and lipids that could be hydrolyzed to sulfate in sediments. Proteins, including the amino acids cysteine and methionine, can account for 20-40% of total organic sulfur in some lake sediments (King and Klug 1982) and may be microbially cleaved to form sulfide via enzymes like cysteine lyase. Oxidized compounds like sulfate esters, which contribute ~35-60% of sedimentary lake organic sulfur, can produce sulfate via aryl sulfatase enzymes (King and Klug 1982). Previous work in low-sulfate rivers (Jiang et al. 2021) and freshwater lakes (Nriagu and Soon 1985; Kokkonen and Tolonen 1987) imply that these sulfate esters, common in lipids and carbohydrates, are likely the dominant form of sedimentary organic sulfur. Sulfonates are typically minor components (King and Klug 1982), but may be amplified in phosphate-starved Lake Superior as microbes substitute sulfate for lipid head groups (Van Mooy et al. 2009). Indeed, initial work in Lake Superior found that <5% of the total seston lipid pool were phospholipids with higher ratios of sulfolipids like SQDG (sulfoquinovosyl diacylglycerol) than marine gyres (Bellinger et al. 2014). Mechanisms for the conversion of sulfolipids to sulfate are less certain as sulfonates and sulfones are resistant to remineralization (Ferdelman et al. 1991). However, some sulfate reducers have been shown to use sulfonates directly as a terminal electron acceptor (Lie et al. 1998). It therefore remains an open question as to which types of organic sulfur are hydrolysable to sulfate in Lake Superior sediments.

Finally, little is known about the fate of sulfide produced during sulfate reduction in Lake Superior sediments. Iron mono- or disulfide formation (e.g., pyrite) is one likely sink, as sediments are rich in iron minerals, reactive iron, and dissolved iron species (Li et al. 2018). Another important sink for sulfides (and polysulfides) may be abiotic organic matter sulfurization – a process known to be important across marine environments (Abdulla et al. 2020; Raven et al. 2021a; Phillips et al. 2022). Notably, sulfurization enhances the preservation of biomarkers (Prahl et al. 1996; Raven et al. 2021b) and the burial of organic carbon (Boussafir and Lallier-Verges 1997; Van Kaam-Peters et al. 1998; Raven et al. 2018), including during ancient low-sulfate regimes (Ma et al. 2021). Initial work on eutrophic sediments implies that sulfurization in lakes is rapid and potentially outcompetes pyritization (Urban et al. 1999; Shawar et al. 2018), but investigations in oligotrophic systems are lacking. Similarly, the role of key sulfur intermediates like elemental sulfur, polysulfides, and thiosulfate remain underexplored and under-characterized in low-sulfate environments.

It is clear from initial investigations and models that Lake Superior hosts a dynamic and active sulfur cycle despite its low sulfate concentrations. Here, we place new constraints on that cycle by isolating and quantifying major pools of organic and inorganic sulfur in the water column and sediments from two contrasting sites in the lake. We track the transformations of organic sulfur from biomass sources in the water to eventual sinks in the sediments. We assess the oxidation states of sulfur in sedimentary pools using X-ray Absorption Spectroscopy/X-ray Fluorescence analysis (XAS/XRF) and identify the active microbial communities in the sediments using shotgun metagenomic sequencing. We also incubate sedimentary microbial communities with organic sulfur compounds to determine their capacity to hydrolyze organic compounds to sulfate. Together, these geochemical and microbiological data provide a holistic characterization of Lake Superior's sedimentary sulfur cycle and offer valuable insights into cryptic organic sulfur cycling in other low-sulfate systems.

Materials and Methods

Site Description

Lake Superior is a deep (~400 m), well-oxygenated oligotrophic freshwater lake with low nitrate (25 µM), phosphate (3 nM), and sulfate (<40 µM) concentrations (Sterner et al. 2007; Sterner 2011; Li et al. 2012). Despite literature references to the lake as "ultraoligotrophic" or "pristine," primary production in the lake is relatively high (9.7 Tg yr^{-1}; (Sterner 2010), supplying most of the organic carbon (~85%) to the water column. Water column dissolved organic matter (DOM) in Lake Superior averages 113 µM (Minor et al. 2019) while particulate organic matter (POM) is <20 µM (Sterner 2011). Although the overall budget of Lake Superior is poorly constrained, an estimated 0.83 Tg yr^{-1} of organic carbon fluxes to sediments. However, the dynamics of carbon burial, sequestration, and remineralization are expected to vary geographically within the lake (Kemp et al. 1978; Johnson et al. 1982). Isle Royale (IR; 47º 58' N, 88º 28' W) and Western Mooring (WM; 47º 58' N, 88º 28' W) are representative anoxic nearshore and oxic offshore sites, respectively (Fig 1a). Compared to WM, sediments at IR have a shallower oxygen penetration depth (~4 vs >10 cm), higher sedimentation rates (0.02 vs <0.01 g cm^{-2} yr^{-1}), higher porewater Fe^{2+} concentrations (30-80 vs <20 µM), and higher maximum TOC (5 vs 2 wt %; Li et al. 2012; Li 2014). WM and IR's distinct geochemistry is apparent in images of cores, which differ in color and location of metal layers (Fig 1b, described further in Li 2014).

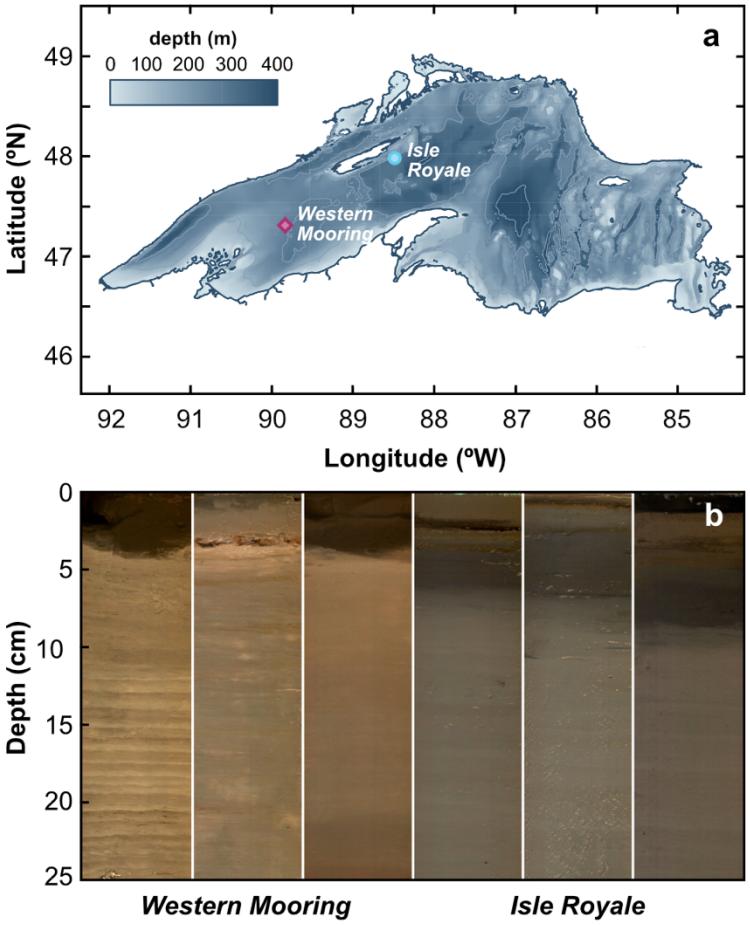

Fig 1. (a) Lake Superior sampling locations. Bathymetry and shoreline data publicly available from NOAA and MNDNR, respectively. Water column and sediment samples were collected at Isle Royale (IR; 47º 58' N, 88º 28' W), marked with a blue circle, and Western Mooring (WM; 47º 58' N, 88º 28' W), marked with a magenta diamond. (b) Images from representative cores at WM and IR to highlight their distinct sedimentology. Photos were re-plotted with permission from the thesis of Li (2014).

Sample Collection

Water column and sediment samples were collected aboard the *R/V Blue Heron* in May and August of 2019 for microbiology and July 2021 for geochemistry. Water column DOM samples were collected with a Niskin rosette outfitted with a SeaBird Model 911 plus CTD at 200 and 235 m at IR and 150 and 180 m at WM. At each depth, 8 L of lake water was gravity filtered through a 0.45 µm Pall capsule filter into acid-washed carboys, acidified to pH 2 with 12 M HCl, and immediately connected to 1 g solid phase extraction cartridges (Bond Elut PPL) following (Dittmar et al. 2008). Sediment sampling followed (Li et al. 2012) using an Ocean Instruments multi-corer (94 mm internal diameter). In 2019, cores were sectioned at 1 cm intervals and aliquots were taken for organic sulfur incubations and shotgun metagenomic sequencing. In 2021, cores were sampled for oxygen penetration depth using a Unisense (Clark-type) microelectrode. Cores for porewater and geochemistry analysis were immediately sectioned in an inflatable glove bag with an N_2 atmosphere in 0.5 cm intervals for the first 3 cm, 1 cm intervals until 15 cm, and 2.5 cm intervals until 20 cm (n=20 samples per core). Samples for geochemistry were stored in pre-combusted glass jars and kept frozen (-20 ˚C) until analysis. Porewater was extracted and transferred into falcon tubes with Rhizons (1 µm membrane pore size) and kept frozen (-80 ˚C) until analysis.

Sediment Incubations

Microbial incubations were conducted by combining ~1 g of IR wet sediments with 9 mL of sterile sulfur-minimal growth media (see SI for recipe). Incubations were supplemented with 10 mM (final concentration) of organic sulfur compounds with varying nominal oxidation states (Vairavamurthy 1998): cysteine (-1), methionine (0), taurine (+4), and sodium dodecyl sulfate (+6). Incubations without sulfur addition served as controls throughout the experiments. Sediments were incubated aerobically, at room temperature (~20 °C) for two weeks in the dark. Post-incubation, tubes were homogenized and subsampled. Sulfate was quantified from treatments and controls with ion chromatography, as described later.

Microbiology Analysis

Total DNA was extracted from 1 g (wet weight) sediment from the 1, 2, 3, 4, 5, and 10 cm sediment horizons with the Qiagen RNeasy PowerSoil DNA elution kit. DNA was quantified with a Qubit v3.0 (Invitrogen) and sent to the University of Minnesota Genomics Center for sequencing. Shotgun metagenome libraries were generated using the Nextera-XT kit (Illumina) and sequenced with Illumina NovaSeq platform with 2x150 basepair reads. Metagenomes were analyzed using methods following Sheik et al. (2022). Briefly, prior to assembly, reads from each shotgun metagenome were quality screened and adapters were trimmed with FastP (Chen et al. 2018). Each sample was individually assembled with MetaSpades (Nurk et al. 2017) to lessen strain level variation that can occur with combined assemblies (Chen et al. 2020). Metagenome assembled genomes (MAGs) were binned using four methods: MetaBat1 (Kang et al. 2015), MetaBat2 (Kang et al. 2019), CONCOCT (Alneberg et al. 2014), and MaxBin2 (Wu et al. 2016). High-quality MAGs were screened from the four assemblies with DASTool (Sieber et al. 2018), de-replicated with dREP (Olm et al. 2017), checked for completion with CheckM (Parks et al. 2015), and taxonomically classified with GTDB-Tk v.95 (Chaumeil et al. 2020). Finally, the abundance and coverage of MAGs were calculated using CoverM (Woodcroft 2023). For high-quality MAGs (completeness >90% and contamination <5%), open reading frames were called with Prodigal (Hyatt et al. 2010), and protein-coding genes were annotated with DRAM (Shaffer et al. 2020).

Porewater Analysis

Reactive thiols were quantified at the University of Minnesota Duluth via fluorescence detection following derivatization with monobromobimane (mBBr). Methods were adapted from Smith et al. (2017): in a glove box, 500 µL of porewater, 10 µL of a 500 mM HEPES / 50 mM EDTA buffer solution and 10 µL of 48 mM mBBr were combined and allowed to react for 30 min before quenching with 25 µL of 4% methanesulfonic acid. Separation of the derivatives proceeded with a HICHROM Prevail C18 column (150 mm x 4.6 mm x 3 µm) on a ThermoScientific Ultimate 3000 UHPLC+ system with a 22-minute gradient using 100% acetonitrile and an aqueous buffer solution (0.1% formic acid, 1% acetonitrile, 98.9% water). The FLD detector operated at an excitation wavelength of 380 nm and an emission wavelength of 480 nm. Retention times for cysteine and sulfide were 2.7 min and 16.2 min, respectively. Glutathione had a retention time of 5.9 min, but co-eluted with excess reagent and could not be quantified. Sulfate, thiosulfate, and sulfite were quantified at UC Santa Barbara on a Metrohm 930 Compact IC (Ion Chromatography) Flex system. Separation proceeded with a 50 min isocratic run (0.7 mL/min flow rate) on a Metrosep A Supp 5 column (250 mm x 4.0 mm x 5 µm) with 0.32 M/0.1 M sodium carbonate/bicarbonate buffer and 2.5% acetone (v/v). Anions were measured via a conductivity detector, with retention times for sulfite, sulfate, and thiosulfate at 26.1 min, 27.5 min, and 42.5 min. Sulfite and thiosulfate were below detection limits in our porewater samples (<1 µM).

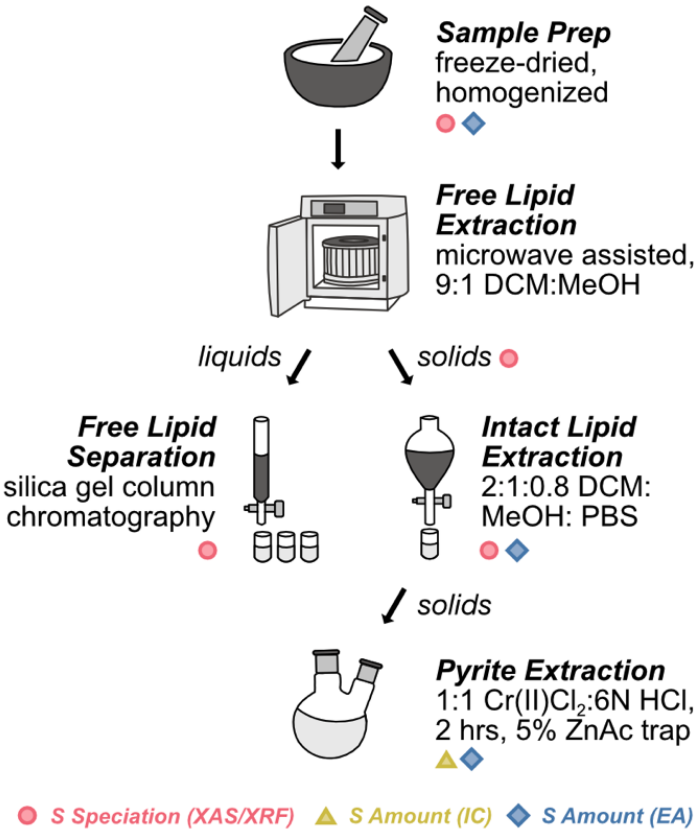

Fig 2. Successive extractions of Lake Superior sediments. Analyses are indicated with pink circles for XAS/XRF, yellow triangles for IC, and blue diamonds for EA. Samples were freeze dried and homogenized. These bulk solids were measured via EA and XAS/XRF. Free lipids were then microwave-extracted. Resulting liquids, containing free lipids and elemental sulfur, were separated on silica gel columns. Redox speciation of sulfur in free lipid fractions was measured via XAS/XRF. Solids following MARS extraction were analyzed with XAS/XRF and then subjected to a modified Bligh and Dyer extraction to isolate intact polar lipids (IPLs). IPLs were measured via EA and XAS/XRF. Remaining solids were subjected to pyrite extraction. Extracted pyrite was quantified by IC and residual sulfur in proto kerogen was quantified by EA.

Geochemical Extractions

Sediments were freeze-dried (72 hrs) prior to homogenization via a Spex 800 Mill (~90 s). Aliquots were set aside for elemental analysis (see below) and bulk characterization of sulfur speciation by XAS/XRF (~1 mg). Bulk XAS/XRF results (Fig S2), notably the absence of detectable iron monosulfide (FeS) in bulk extracts, were used to optimize the extraction scheme to isolate various organic sulfur and carbon pools (Fig 2). First, ~4 g aliquots were microwave-extracted with a MARS-6 (CEM) in 20 mL of 9:1 dichloromethane: methanol (DCM: MeOH). Liquid and solid phases were separated via vacuum filtration on pre-combusted GF/F filters. Filtrates were further separated on 1 g silica gel columns. Briefly, elemental sulfur (S^0) was eluted with 10 mL 4:1 hexane: DCM and free lipids with 10 mL of 1:1 DCM: MeOH. S^0 was measured by mass difference before and after exposure to activated copper. Free lipids were concentrated in DCM (~100 µL) and aliquots (~10 µL) were plated dropwise on quartz slides for XAS/XRF analysis. Solids remaining after MARS extraction were subjected to a modified Bligh and Dyer extraction with 2:1:0.8 DCM: MeOH: PBS to isolate intact polar lipids (IPLs) and other intermediate polarity compounds (Bligh and Dyer 1959; Bellinger et al. 2014). This extract was aliquoted for EA and XAS/XRF measurements. The remaining solids were transferred to a round bottom flask with 30 mL of 1:1 chromium (II) chloride: 6N hydrochloric acid solution under an N_2 atmosphere to extract pyrite (2 hrs, 70 ˚C). Volatilized sulfide passed through a condenser and was trapped as ZnS by sparging with 5% m/v zinc acetate solution. Zinc sulfides were washed and then oxidized to sulfate via two successive reactions with 1 mL hydrogen peroxide (24 hrs, 60 ˚C). Sulfate abundance was measured by IC as described above for porewater sulfate. Residual sediments, containing silicates and "proto kerogen," were rinsed of residual $CrCl_2$, dried overnight in an oven at 70 ºC, and aliquoted (~30 mg) for C/S content determination via elemental analysis (below).

Elemental Analysis

Carbon and sulfur contents of bulk sediments, pooled IPLs, and proto kerogen were quantified by elemental analysis (EA). Sediment samples were prepared with ~0.5 mg tungsten (III) oxide (W_2O_3) to aid combustion. Polar lipids were pooled across three depth horizons to ensure adequate signal-to-noise ratios. Analyses were conducted on an Elementar Vario Isotope Select Elemental Analyzer (EA) with a He carrier (200 mL/min). The desorption column released CO_2 at 90 ˚C and SO_2 at 250 ˚C for quantification by thermal conductivity detector (TCD; Raven et al. 2020; Phillips et al. 2021). Elemental abundances were calibrated using a sulfanilamide standard curve (10 – 200 µg S, 20 – 400 µg C), which was run in duplicate each day ($R^2 > 0.9990$).

Sulfur Speciation

Sulfur K-edge X-ray absorption / X-ray fluorescence (XAS/XRF) spectra were collected at the Stanford Synchrotron Radiation Lightsource (SSRL) on beam line 14–3, which uses a Si (111) (Φ = 90) double crystal monochromator for beam energies from 2460 to 2540 eV, which are calibrated to the thiol pre-edge peak of thiosulfate at 2472.02 eV. The X-ray beam was trimmed to a size of 500 x 500 µm at a flux of ~$8*10^{10}$ photons per second to yield 'bulk' compositions of extracts and residues. XAS/XRF spectra were processed with SIXPACK (Webb) using a K-edge E0 of 2473, variable pre- and post-edge linear normalization ranges to achieve stable baselines, and a variety of organic sulfur standards across oxidation states (Table S1, Fig 3; Raven et al. 2021a). Inorganic standards used for bulk sediments included elemental sulfur, pyrite, pyrrhotite, anhydrite, and seawater sulfate. Relative abundances of sulfur species were calculated based on linear deconvolution fitting of these standard spectra (see SI data file).

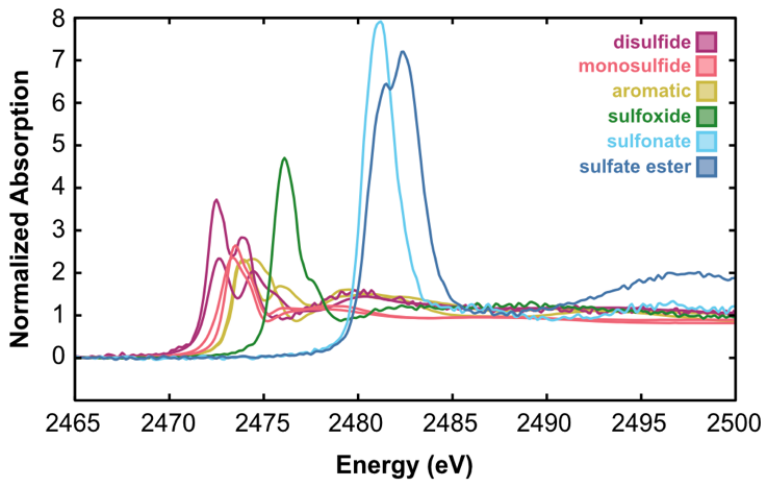

Fig 3. Spectra of organic sulfur standards used for XAS/XRF data processing. Note the relationship between oxidation state of the sulfur atom and energy level of maximum absorption: reduced species like disulfides (magenta), monosulfides (pink), and aromatic sulfur (yellow) have lower eV level peaks, while oxidized organic sulfur like sulfoxides (green), sulfonates (light blue), and sulfate esters (blue) absorb at higher energies. Disulfide and monosulfide standards were pooled in analyses.

Results

Sediment Incubations

IR sediments were used to create oxic microcosm incubations, amended with 10 mM concentrations of biologically relevant organic sulfur compounds across oxidation state and degradation pathway. These incubations aimed to assess if *in situ* microorganisms were able to degrade the organic sulfur substrate and produce sulfate (Fig 4). The control microcosms, which contained no added substrate, had no significant sulfate production with depth. The sulfonic acid taurine had the highest sulfate production regardless of depth followed by the sulfate ester sodium dodecyl sulfate. In contrast, cysteine, and methionine produced low and sporadic sulfate: Cysteine addition led to sulfate accumulation in the upper sediment (0-3 cm), while methionine had two zones (2-5 cm, 6-8 cm). Notably, sulfate production was only statistically different from the control with depth for SDS and taurine ($p < 0.001$; Dunn's Kruskal-Wallis test), but not methionine ($p = 0.06$) or cysteine ($p = 0.07$).

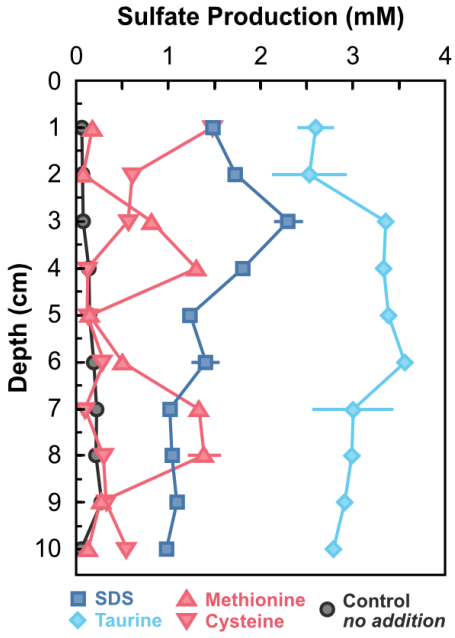

Fig 4. Sulfate accumulation during incubations of inoculates from discrete depths of IR sediments, with added organic sulfur. Substrates included the sulfate ester SDS (sodium dodecyl sulfate) in dark blue squares, the sulfonic acid taurine in light blue diamonds, and the mono sulfides cysteine and methionine in regular and inverted pink triangles, respectively. Incubations were run in duplicates, with 1σ standard deviations shown in error bars.

Microbial Community

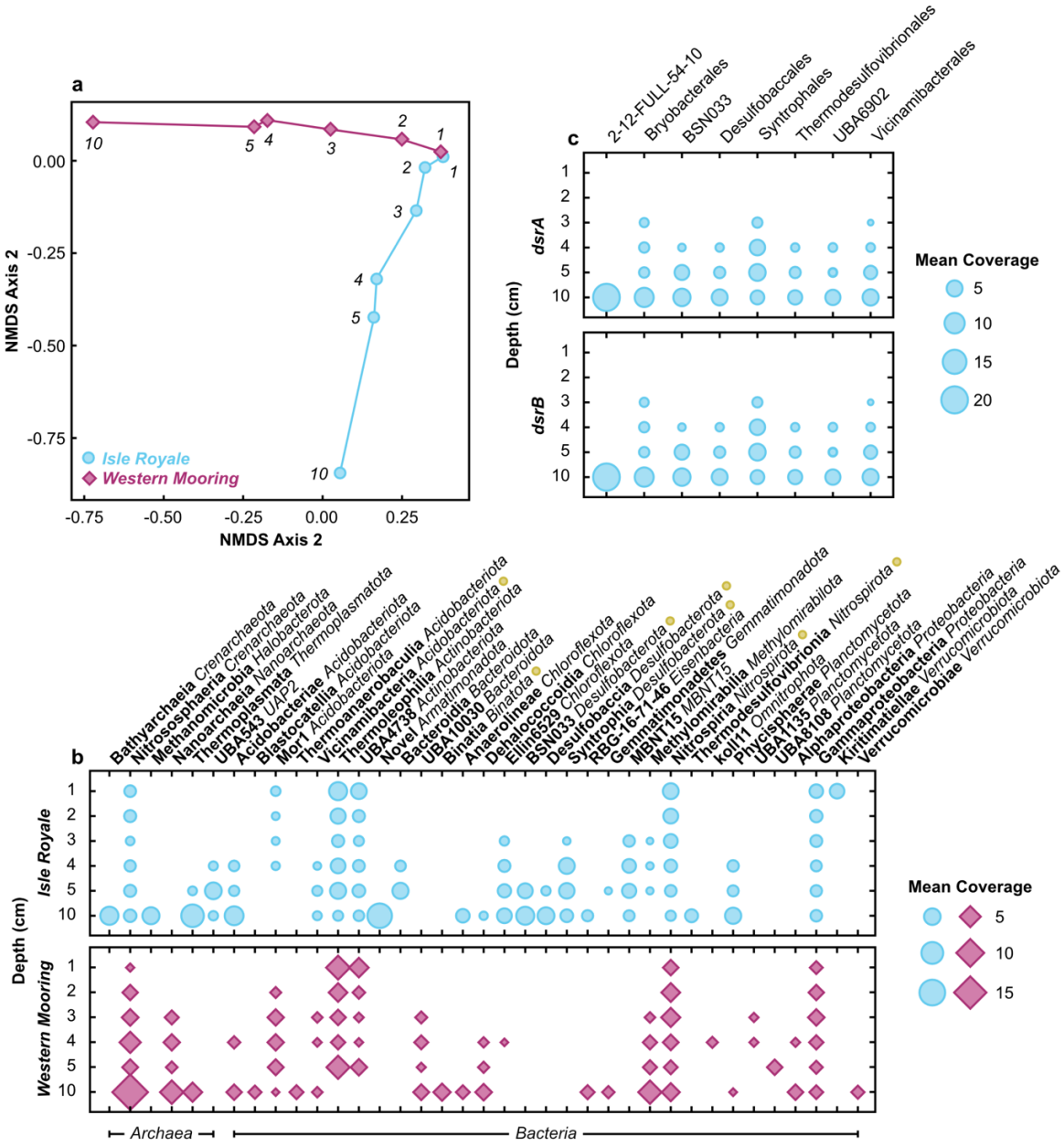

Fig 5 (a) A Nonmetric Multidimensional Scaling (NMDS) plot of the community structure from both stations. Numbers next to the points are the corresponding depths (cm) from where that sample originated. (b) Taxonomic distribution of Metagenomic Assembled Genomes (MAGs) from the 16S rRNA gene amplicon at both Isle Royale and Western Mooring with depth. MAG taxonomy is at the class level, with phyla in italics. MAGs are organized alphabetically from left to right by phyla. To understand key players across stations, only MAGs that were >1% abundance are included. Yellow dots indicate the classes that correspond to orders detected in panel c. (c) Distribution of dsrA and dsrB genes with depth in MAGs in Isle Royale at the order level. For b and c, the size of the points is scaled by the mean coverage of each MAG within the phylogenetic cutoff.

Metagenome Assembled Genome (MAG) abundance was used to assess microbial community composition differences across stations (Fig 5). Non-metric multidimensional scaling (NMDS)

indicated that the microbial communities in surface sediments (1 cm) from IR and WM were similar, but quickly diverged with depth (Fig 5a). While a full examination of microbial community composition and capabilities is beyond the scope of this paper, an examination of abundant (>1% coverage) Archaea and Bacteria revealed differences in taxa at WM and IR with depth and drove observed community differences (Fig 5b). Many of the microorganisms recovered from both stations were novel at the family, genus, and species levels and we therefore visualized results by class. A total of 37 classes were detected in IR and WM with average coverage >1%, although only three were >10% in any sample (Thermoplasmatota, Nitrososphaeria, and a novel Armatimonadota). Further details on the remaining classes, except sulfate reducers (see below) can be found in the SI. Notably, IR taxa tended to be abundant either above or below the oxycline (~4 cm), while distributions were more even in WM.

Desulfobacterota (formerly Deltaproteobacteria) were only identified in IR sediments below the oxycline and included uncultured representatives of BSN033, Desulfobaccia, and Syntrophia. Together, these three Desulfobacterota classes accounted for 14% of the microbial community at 10 cm in IR. The presence of Desulfobacterota suggested that sulfate-reducing bacteria may be present at IR. Using MAG gene annotations from DRAM, we searched for the dissimilatory sulfite reductase (*dsrAB*) genes that mediate the reduction of sulfite and/or oxidation of sulfide. In our MAGs, we found that *dsrAB* was only present at station IR below the oxycline. In total, we detected eight MAGS from eight orders with *dsrAB* (Fig 5c), seven of which were in classes that were >1% abundance in at least one sample (Fig 5b, yellow dots). Three of these MAGs were within the Desulfobacterota phylum*:* BSN033 (family *BSN033*), Desulfobaccales (family *0-14-0-80-60-11*) and Syntrophales (family *UBA5619*). Additionally, we found two Nitrospirota: Thermodesulfovibrionales (family *SM23-25*) and UBA6902 (family *UBA6902*). Two Acidobacteriota MAGs were also detected with *dsrAB*: Vicinamibacterales and Bryobacterales. The latter of which, in class Terriglobia, was below our cutoff for visualizing the microbial community (< 1% relative abundance). Finally, we identified 2-12-FULL-54-10 within Binatota – notably this microbe, although containing *dsrAB*, was <1% abundance in IR deep sediments but 3% at 10 cm in WM.

Porewater Sulfur

Porewater sulfate profiles (Fig 6a) revealed a clear contrast between the two sites. At IR, porewater sulfate concentrations increased from the surface (21 μM) to a maximum at 2–3 cm depth (51 μM) and then decreased to zero by 8 cm. At well-oxygenated WM, surface sulfate concentrations were higher (29 μM) but decreased to only 17 μM with depth. Sulfide was not detected in the deeply oxygenated WM sediment, but at IR, sulfide reached a maximum of 36 nM near the oxygen penetration depth (~4 cm; Fig 6b). Porewater cysteine distributions in IR resembled sulfide, with a maximum concentration of 70 nM at 5–6 cm depth and a secondary peak at 3–4 cm depth (Fig 6c). In WM sediments, porewater cysteine was highest at the sediment-water interface (21 nM) but remained <10 nM in deeper sediments.

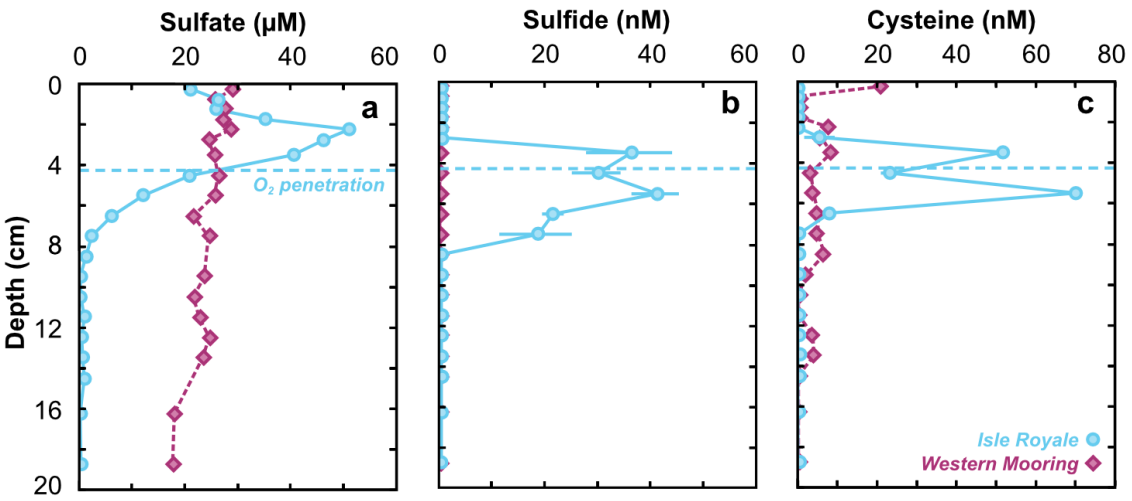

Fig. 6. Porewater (a) sulfate (b) sulfide and (c) free cysteine measured from Isle Royale (IR; (blue circles) and Western Mooring (WM; magenta diamonds) sediments. The light blue dashed line represents the approximate oxygen penetration depth in IR, measured by microprobe in a duplicate core. Dissolved O_2 in WM remains ≥ 38 μM to 9 cm depth (measurement depths were limited due to probe length) and is assumed to be oxic throughout. Error bars represent 1σ standard deviations of replicates of standards at similar concentrations.

Solid Phase Sulfur

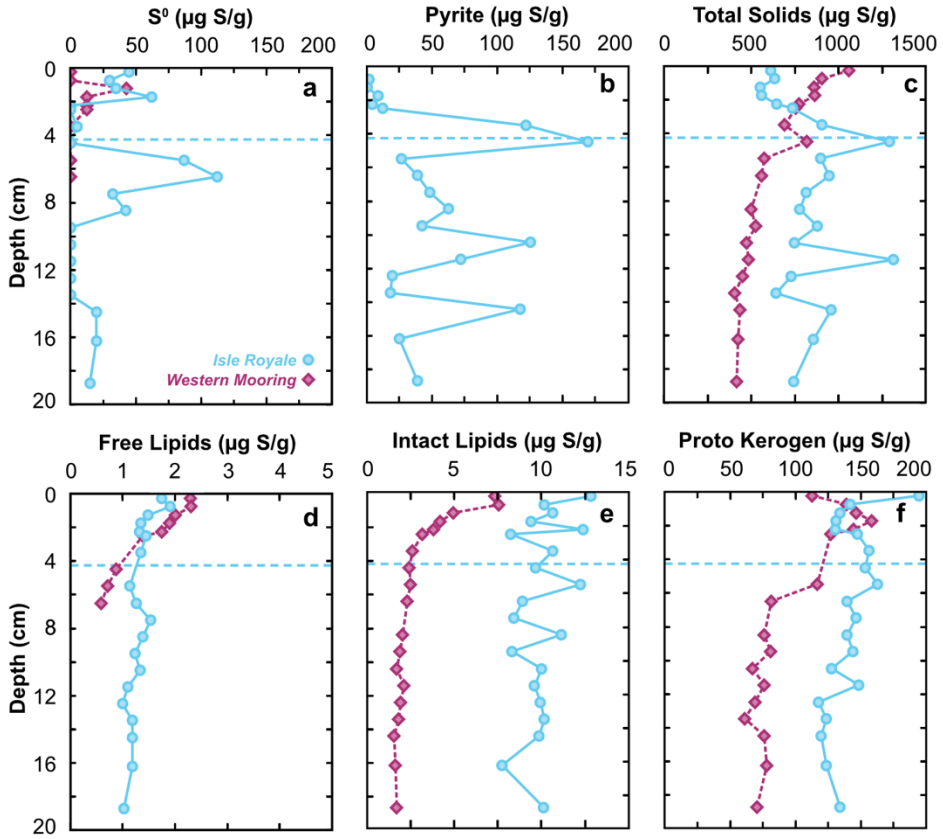

Fig 7. Solid phase sulfur pools from Lake Superior sediments including (a) elemental sulfur, (b) pyrite, (c) total solid phase S, (d) free lipids, (e) polar lipids, and (f) residual proto kerogen following lipid and pyrite extractions. IR samples are shown with light blue circles, with oxygen penetration depth for reference. WM is seen in magenta diamonds. All are plotted per gram of dry sediment. See SI data file for all geochemical data.

Both organic and inorganic solid sulfur phases were measured in Lake Superior sediments (Fig 7). A subtle peak in elemental sulfur concentrations (43–62 μg S/g) was present at 1–2 cm depth at both sites (Fig 7a). In deeper sediments, elemental sulfur was more abundant at IR than at WM, reaching a maximum concentration of 112 μg S/g at 6-7 cm depth. Pyrite in IR sediments (defined as CRS extracted) was not detectable (~<0.001 ppm) in WM but was present throughout all but the shallowest 3 cm of IR sediment (Fig 7b). Here, pyrite concentrations had several distinct peaks, reaching a maximum concentration of 169 μg S/g near the oxygen penetration depth. Bulk sediment C:S ratios and sulfur weight percentages were used to calculate total sedimentary sulfur (Fig 7c). Total sulfur was higher on average in IR (893 μg S/g ± 197) than WM (520 μg S/g ± 120) with depth and had peaks that paralleled other solid phase maxima.

Concentrations of sulfur in lipid pools were calculated from extract masses using molar S:C ratios. For intact polar lipids, molar C:S ratios were measured on pooled samples, yielding average values of 81 ± 13 in IR and 285 ± 9 in WM. Molar C:S ratios in free lipids were assumed to be approximately 100 (Moran and Durham 2019). Total free lipid sulfur in IR and WM were similar at the surface (~ 2 μg S/g) and throughout the uppermost (oxygenated) sediments (Fig 7d). Below 4 cm, free lipid sulfur remained relatively constant at IR (averaging 1.2 μg S/g) but decreased in WM. Intact polar lipids were extracted after free lipids and contained more sulfur overall (Fig 7e). Unlike free lipids, the two sites had different initial concentrations of sulfur in IPLs: 12.9 μg S/g at IR and 7.4 μg S/g at WM. Concentrations of sulfur in IPLs declined over the upper 4 cm at WM but not at IR. IPL sulfur concentrations averaged 10 ± 1.4 (1σ) μg S/g in IR sediments and averaged 2.0 ± 0.3 μg S/g below 4 cm depth at WM.

Solid phase sulfur following lipid, pyrite, and elemental sulfur extractions was operationally defined as proto kerogen and calculated from remaining sediment masses and molar C:S ratios (Fig 7f). Like other solid phase pools, there was more sulfur in IR: proto kerogen averaged 138 μg S/g ± 13 after a surface peak of 195 μg S/g. Meanwhile, proto kerogen in WM had a sub-surface peak of 159 μg S/g, but decreased to an average of 78 μg S/g (± 14) below 5 cm.

Given previously published porosity measurements (Li et al. 2012), we calculated that solid phase sulfur accounted for ~99% of total sulfur, with porewater sulfur at most 1% of the mass balance (see SI data file) – and only at the sediment-water interface. Below this, porewater sulfur (Fig 6) was on average ~0.3% of total sedimentary sulfur. Of the sedimentary sulfur pools, proto kerogen is the primary component of the sulfur budget at both sites (Fig S1, Fig 7). At IR only, inorganic sulfur (i.e., pyrite and elemental sulfur) is similar to proto kerogen concentrations in deeper sediments. Total sedimentary sulfur at IR is elevated at several depths with abundant pyrite. Free and intact lipids were ~1-2% of total sulfur in IR and ~0.5% in WM.

Sulfur Speciation

We assessed the oxidation state and chemical speciation of sulfur in water column DOM, bulk sediment, free lipids, and IPLs using XAS/XRF. XAS/XRF spectra could not be collected on proto kerogen due to its low concentration against the scatter from sedimentary silicates. For both WM and IR, a majority (~90%) of DOM was either highly oxidized (sulfate esters, sulfonic acids/sulfonate) or moderately oxidized (aromatics, sulfoxides), with minimal contributions from reduced compounds (mono or disulfides; Fig S3). Results for bulk sediments (Fig S2) indicated no significant iron monosulfides, obviating the need for acid-volatile sulfur extraction. Near the

sediment-water interface for both IR and WM, most (~80%) of total sedimentary organic sulfur was intermediate or oxidized, in the forms of sulfonic acids, sulfate esters, and sulfonates. Bulk sedimentary sulfur speciation in WM was largely constant with depth, but the relative amounts of disulfides and monosulfides increased with depth in IR.

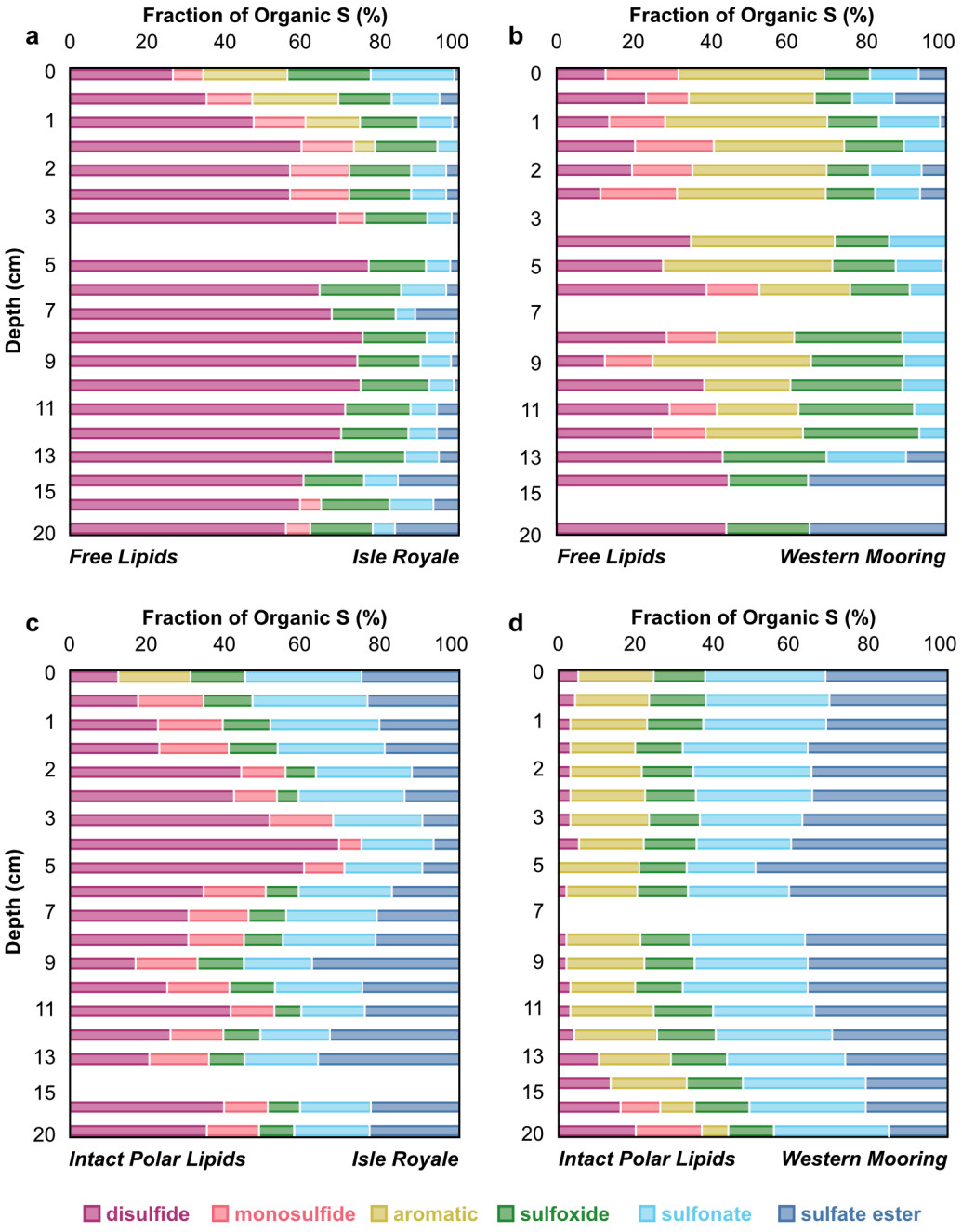

Fig 8. Sulfur speciation as inferred by XAS/XRF spectra for (a) IR free lipids, (b) WM free lipids, (c) IR intact polar lipids, and (d) WM intact polar lipids. Each spectrum was fit with various organic sulfur standards, with disulfides in magenta, alkyl monosulfides in pink, aromatics in yellow, sulfoxides in green, sulfonates/sulfonic acids in light blue, and sulfate esters in dark blue. Stacked spectra and plots

of individual components with depth can be found in the SI (Figs S4-5). Note that the y-axis is non-linear due to higher sample resolution in surface sediments.

A similar pattern was seen in free and intact lipid extractions (Fig 8, S4-5), with higher reduced sulfur content in IR than WM. Free lipids from IR (Fig 8a) were predominantly disulfide, averaging 68% below the oxycline. In contrast, sulfur in WM free lipids (Fig 8b) was 27% disulfide. Sulfoxides represented a small (~10%) yet consistent component of free lipids from each site. The relative abundance of aromatics and monosulfides were low and constrained to surface sediments in IR free lipids. In WM, however, monosulfides and aromatics were more consistent – and in the case of aromatics, more abundant (~30%) – with depth. Oxidized species like sulfonates and sulfate esters were unsurprisingly low in free (relatively nonpolar) lipid pools. Instead, intact polar lipids (Fig 8c-d) had more oxidized organic sulfur. Sulfonates comprised an average of 23% of total sulfur in IR and 29% in WM, while sulfate esters were 21% and 33% of intact lipid sulfur, respectively. Intermediate compounds, including aromatic sulfur and sulfoxides, were elevated in WM intact lipids compared to IR. For example, IR only had detectable aromatic sulfur in intact lipids at the sediment water interface, but aromatics were ~18% of intact lipid sulfur with depth in WM.

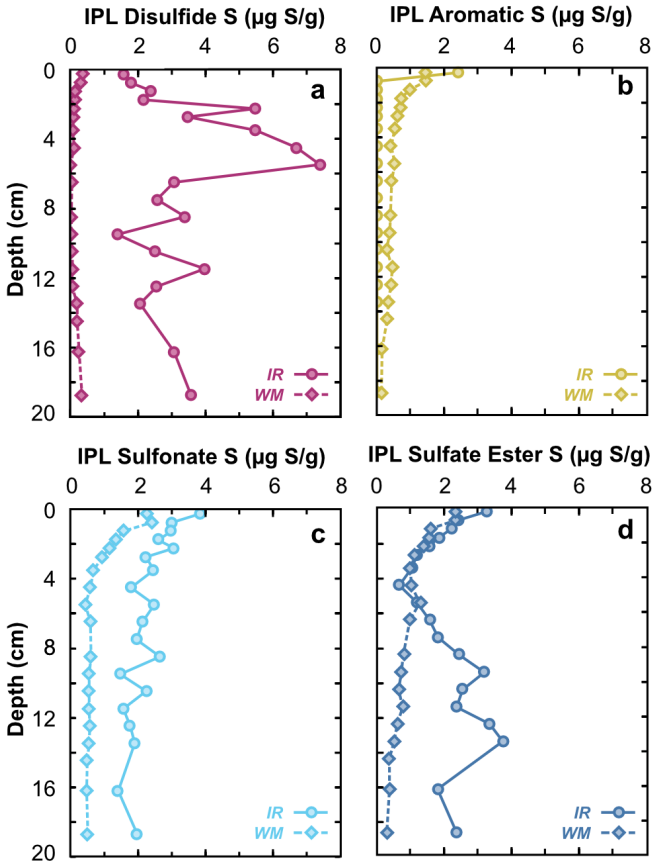

Fig 9. Sulfur accumulation in IR (solid lines, circles) and WM (dashed lines, diamonds) in selected intact polar lipid (IPL) pools, including a) disulfides (magenta), b) aromatics (yellow), c) sulfonates (light blue) and d) sulfate esters (dark blue). All units are in µg of S per gram of dry sediment, as calculated from a combination of XRS/XRF spectra, molar C:S ratios, and measured masses following extractions. Note that the x axis is maintained to allow comparison.

Finally, disulfides in WM intact lipids were significantly lower (~6%) than in IR, where disulfides peaked at 69% abundance at 4 cm. Given our sedimentary mass balance (Fig 7, S1), we calculated the absolute, rather than relative, accumulation of sulfur within intact lipid extract pools (Fig 9). Across all sulfur redox states, sulfur concentrations are initially ~2x higher in IR than WM – except

for disulfides, which are ~5x greater (Fig 9a). By 5 cm, intact lipid disulfides reach a maximum of 7.4 µg of S per g of sediment, coinciding with peaks of pyrite and elemental sulfur (Fig S7). Aromatic and sulfonate sulfur, in both IR and WM, displayed characteristic exponential degradation. Sulfate ester sulfur within IR's intact lipids, however, had a broad, sub-surface peak ~4 µg S per g of sediment.

Discussion

Lake Superior's microbial community includes sulfate reducers

No studies have surveyed the sedimentary microbial community in Lake Superior beyond specific cycles like iron (Dittrich et al. 2015) and nitrogen (Small et al. 2016; Crowe et al. 2017). Although a full metabolic examination is beyond the scope of this paper, we provide a broad overview of the bacteria and archaea in WM and IR identified by our metagenomic sequencing. Many taxa were detected at IR and WM that degrade various organic matter pools, including within Acidobacteriota and Chloroflexi. These phyla are extremely metabolically diverse and are not uncommon in lake sediments (Davis et al. 2011). Chloroflexi, especially classes observed here like Anaerolineae and Dehalococcoidia, are important initial fermenters for complex compounds (Suominen et al. 2021). Meanwhile, many Verrucomicrobiota may be specialists (Williams et al. 2021), for example by consuming sulfated polysaccharides (Orellana et al. 2022) that appear to be concentrated in Lake Superior sediments (Fig 9d). Acidobacteria, including observed Pyrinomonadaceae within Blastocatellia, are also carbon degraders (Ivanova et al. 2020). This highlights that Lake Superior sediments, like other marine and freshwater systems, harbor diverse heterotrophic communities that drive carbon mineralization and likely fermentation processes.

Microbial community composition in surface sediments was similar between IR and WM (Fig 5a), a phenomenon driven by a few dominant taxa that co-occurred at both stations. These included the Nitrososphaeria within the Crenarchaeota phylum, a common group of ammonia-oxidizing Archaea that have been previously identified in Lake Superior via ammonia monooxygenase (*amoA*) gene surveys (Bollmann et al. 2014). Co-occurring bacterial classes in surface sediments included Themoleophilia and UBA3748 within the phylum Actinobacteria – a primitive and ecologically significant lineage characterized by diverse metabolisms (Shivlata and Satyanarayana 2015). Nirtospiria, a class of nitrite oxidizers, and Gammaproteobacteria, a class of mostly heterotrophic bacteria, were also abundant in the surface microbial communities of both IR and WM. Lake Superior's surface communities, overall, represent a complex consortium of carbon and nitrogen cyclers.

While many co-occurring surficial groups remained abundant with depth, divergence in community composition was driven by non-co-occurring groups, especially sulfur cyclers. Uniquely in WM, we saw classes of Nanoarchaeia, an obligate Archaeal syntroph, and UBA10030, a complex organic matter degrader, become abundant with depth. In IR, however, there were clear shifts to anaerobic metabolisms, with the rise of taxa like Bacteroidia, BSN033, Desulfobaccia, Syntrophia, and MBNT15. Indeed, most of the classes unique to down-core IR sediments contained dissimilatory sulfite reductase (*dsrAB*) genes (Fig 5c), the appearance of which coincided with porewater sulfide production ~4 cm (Fig 6b). In total, we identified eight *dsrAB*-containing taxa, which accounted for ~20% of IR's 10 cm sedimentary community. Most (14%) of this sulfate reducing community were canonical Desulfobacterota. Other sulfate reducers

included Thermodesulfovibrionales, which have been previously found in freshwater, iron-rich lake sediments (Elul et al. 2021). We also identified *dsrAB* in thus-far uncultured Binatota, which appears to be genetically capable of degrading simple methane sulfones and sulfides (Murphy et al. 2023). We also find sulfate reducing Acidobacteria, which are often overlooked for their sulfur cycling potential despite accounting for the second-highest number of *dsrAB* hits in marine sediments (Flieder et al. 2021). Taken together, we provide evidence that sulfate reduction is a key metabolism in anoxic Lake Superior sediments.

Other metabolisms involving iron or sulfur may also drive community differences in IR sediments below the oxycline. Concentrations of dissolved sulfur intermediates involved in disproportionation (e.g., thiosulfate) were below detection limits (<1 μM), but solid-phase elemental sulfur concentrations reached 3.5 μmol S/g (112 ug S/g sediment; Fig 7a). Due to very low (<40 nM) sulfide (Fig 6b), elemental sulfur disproportionation would be energetically favorable near IR's oxygen penetration depth (Finster 2008). Notably, organisms with *dsrAB* genes are not necessarily restricted to sulfate reduction and may grow via disproportionation (van Vliet et al. 2021) – for example our identified Thermodesulfovibrionia (Umezawa et al. 2021). Despite documented Fe^{2+} accumulation in IR porewaters below ~5 cm (Li et al. 2012), canonical iron reducers like Geobacter and Shewanella were not >1% abundance. However, previous metagenomic investigations of iron layers in Lake Superior have implicated Nitrospiria (Dittrich et al. 2015), an abundant taxon at IR and WM in our dataset. Future work should continue to catalog the diverse metabolisms in Lake Superior sediments with metagenomics and transcriptomics to better understand the energetics of iron metabolisms relative to microbial sulfur reduction.

Oxidized organic sulfur likely fuels Lake Superior sulfate reduction

In low-sulfate environments, organic sulfur may dwarf inorganic reservoirs and actively drive sulfur transformations (Fakhraee and Katsev 2019). In Lake Superior we find that even at sulfate peaks (51 μM; Fig 6a), organic sulfur concentrations are two orders of magnitude higher (Fig 7; SI Data File). Under these conditions, models suggest that up to 50% of sulfate reduction may be supported by the hydrolysis of organic sulfur compounds to sulfate (Fakhraee et al. 2017). Our study sought to confirm the potential of organic sulfur to act as a fuel for sulfate reduction. We also aimed to better characterize the redox state of the organic sulfur involved, as both reduced thiols from proteins and oxidized sulfate esters and sulfonates from lipid/polysaccharide pools have been hypothesized as potential precursors (Bellinger et al. 2014; Fakhraee et al. 2017).

One potential sulfate source is protein-derived amino acids, namely the thiol cysteine (R-SH) and the monosulfide methionine (R-S-CH_3). Oxidative cysteine and methionine lyase enzymes can sever carbon-sulfur bonds, producing free thiols and methanethiols, respectively. In the presence of O_2, free thiols would readily oxidize to sulfate while methanethiols would likely be consumed – for example by Binatota sulfate reducers observed in IR (Murphy et al. 2023). Incubation results hint at some microbial capacity to generate sulfate from these amino acids (Fig 4), although maximum production did not correlate with observed porewater sulfate peaks ~2-3 cm (Fig 6a). Porewater cysteine peaks were also low and offset from sulfate, with maximums below the oxycline (Fig 6c). Further, we see little evidence of a large pool of amino acid sulfur in our sulfur speciation dataset. Deep water column DOM (Fig S3) is at most 10% reduced compounds like monosulfides. While DOM is not an ideal proxy for organic matter delivered to sediments, it can

still help inform our understanding of organic sulfur in primary producers (Beaupré 2015). Bulk sediments and proto kerogen (inferred by subtraction) also have low relative abundance of monosulfides (Fig S2). Although these low cysteine and methionine abundances do not preclude the possibility of rapid, active cycling, we hypothesize that sinks other than hydrolysis are more likely keeping amino acid concentrations low. First, cysteine and methionine rapidly oxidize to intermediate oxidization sulfoxides and sulfones (Phillips et al. 2021; Silverman et al. 2022), which we observe throughout our speciation data. Second, many heterotrophs can directly incorporate free amino acids into proteins. While we cannot completely disregard reduced sulfur as a potential sulfate precursor, we conclude that it is most likely a minor contributor.

We instead turn to the potential role of oxidized organic sulfur in Lake Superior sediments. Lipids and polysaccharides contain oxidized sulfur that is carbon bound like sulfonates ($R\text{-}SO_3$) or non-carbon-bound sulfate esters ($R\text{-}O\text{-}SO_3\text{-}H$). Sulfate esters are readily hydrolyzed to sulfate via widely distributed aryl sulfatases (Roy 1971). A diverse suite of enzymes aids the conversion of sulfonates to sulfate, although genetic work has mostly focused on model C_2-C_3 compounds like taurine (Durham et al. 2015; Xing et al. 2019). Notably, Lake Superior's active heterotrophic microbial community may play a role in breaking down complex sulfonates like SQDG into smaller, hydrolysable pieces. Incubations with IR sediments revealed a high capacity for these transformations; samples amended with SDS, a model sulfate ester, yielded significant sulfate production, although the highest concentrations were observed with taurine addition (Fig 4). Our speciation data also highlighted the prevalence of oxidized organic sulfur across major pools: sulfonates and sulfate esters accounted for 60% of DOM (Fig S3), 40% of bulk sediments (Fig S2), 50% of intact polar lipids (Fig 8, S5), and 70% of sediments following lipid extraction (SI Data File). Remarkably, intact lipids were 1-2% of the total sedimentary sulfur budget (Fig S1) – likely partially reflecting elevated water column SQDG production under phosphate starvation (Bellinger et al. 2014). These results implicate oxidized sulfur in fueling Lake Superior sulfate reduction.

Our results have implications beyond our case study in Lake Superior. Organic sulfur may play an active role in inorganic nutrient cycles across other sulfate-starved systems like oligotrophic soils, the deep subsurface, or the Archean Ocean. In these environments, oxidized organic sulfur like sulfonates and sulfate esters are likely an overlooked source of sulfate (Fitzgerald 1976). Future work should continue to catalog sulfur oxidation states in organic matter and leverage metagenomics to track specific catabolic pathways of oxidized sulfur compounds like SQDG.

Pyritization and organic matter sulfurization are co-occurring sulfide sinks

Models of porewater sulfide in Lake Superior predicted accumulation to ~10 μM (Fakhraee et al. 2017), but we observed three orders of magnitude lower concentrations (40 nM) in Lake Superior sediments (Fig 6b), suggesting highly efficient sulfide sinks in IR sediments. The canonical sink for sulfide in anoxic sediments is pyrite formation (FeS_2; Canfield 2001), which requires various inorganic iron and sulfur ingredients. Previous work at IR found high concentrations (30-80 μM) of dissolved Fe^{2+} below ~4 cm, the seasonal oxycline. This down-core accumulation of Fe^{2+} was attributed to microbial iron reduction of abundant Fe(III) minerals in the Lake Superior watershed (Sterner 2010; Dittrich et al. 2015). The initial products in the reactions of Fe(III) minerals and dissolved sulfide are likely Fe^{2+} and elemental sulfur, which can then co-precipitate to form FeS. FeS is considered an intermediate, requiring another reaction for conversion to pyrite (Rickard and

Luther 2007): Although we do not observe FeS directly (via XAS/XRF) in our bulk sediments (Fig S2), elemental S is abundant and available to support the conversion of FeS to FeS_2 in IR sediments at 3–7 cm depth (Fig 7a, S1). Elemental S decreases below detection limits in underlying sediments, possibly kept low by pyrite formation, microbial oxidation/disproportionation, formation of polysulfides, or a mixture of these reactions.

We observe maximum (169 µg S/ g) pyrite concentrations at 4-5 cm (Fig 7b). At this interval, pyrite is nearly equal to the proto kerogen sulfur pool (Fig S1) and accounts for 13% of the total sulfur mass balance (SI Data File). In deeper IR sediments, pyrite concentrations vary by nearly an order of magnitude, ranging from 17.5 – 125 µg S/ g sediment – a feature that is replicated by an independent measurement via XAS/XRF (Fig S6). These layers of abundant pyrite likely represent the reduced products of past mm-scale accumulations of Fe(III) minerals, which may have marked the historical positions of the O_2 penetration depth (Li and Katsev 2014; Dittrich et al. 2015). Pyrite records and their isotopes are widely used to reconstruct paleoenvironments and changes in local geochemistry, with the general assumption that they reflect the integrated signal of continuous pyrite formation over some sulfidic interval in the water column and/or sediments (Jørgensen 1979). Our results emphasize that pyrite formation in low-sulfate systems may reflect processes and fluxes at a very specific location within the sedimentary environment like the oxycline (Gomes et al. 2022) – a framework that may substantially impact interpretations of freshwater pyrite records (Davison et al. 1985). For example, sulfate released from organic matter via hydrolysis could pin porewater sulfate isotopes near biomass values (thus resisting Rayleigh fractionation) in the zone of pyrite formation. This would yield pyrite with consistent, ^{34}S-depleted, "open-system" type sulfur isotope signals (Bottrell and Raiswell 2000) despite its formation several centimeters deep in the sediments.

A second, concurrent sink for sulfides in IR sediments appears to be organic matter sulfurization, where sulfides and polysulfides attack functional groups to create new carbon-sulfur bonds (Kohnen et al. 1989; Shawar et al. 2018) and generate alkyl mono- and di-sulfides (van Dongen et al. 2003; Amrani and Aizenshtat 2004; Raven et al. 2021a). Polysulfides form spontaneously in the presence of sulfide and elemental sulfur and are therefore predicted to occur in IR sediments where those species overlap (4–8 cm depth; Figs 6-7). Organic materials that are polymerized via sulfurization also appear to be relatively resistant to microbial degradation and therefore enhance carbon burial over geologic time (Boussafir et al. 1995; Boussafir and Lallier-Verges 1997; Sinninghe Damsté et al. 1998). The most compelling evidence for organic matter sulfurization in Lake Superior is the accumulation of up to 8 µg of disulfide S per g of sediment in IR intact lipids (Fig 9a). This peak in organic disulfide abundance occurs in the same depth interval (4–5 cm) as peak concentrations of sulfide, pyrite, and elemental sulfur (Fig S7). This pattern clearly contrasts the depth trends seen in other forms of lipid sulfur, which suggest gradual loss over time (Fig 9). Disulfides were also relatively abundant (~60-70% of total free lipid sulfur) with depth in IR, especially versus the "control" site WM (20-30%). Total lipid sulfur accounted for ~1-2% of the solid phase sulfur mass balance (Fig S1) and at some depths rivaled pyrite concentrations. Our 20 cm cores represent ~400 years of diagenesis (Kemp et al. 1978; Li et al. 2012), implying lipid sulfurization on a decadal timescale. This is consistent with studies of rapid polysulfide sulfurization in aquatic sediments and laboratory experiments (Francois 1987; Kok et al. 2000; van Dongen et al. 2003; Amrani et al. 2008).

Taken together, we observe concurrent, efficient sinks for sulfide produced from microbial sulfate reduction in the form of pyritization and organic matter sulfurization. Both pyrite and sulfurized lipids form immediately below the oxycline, at ~4-5 cm. This conclusion bypasses the traditional narrative for high-sulfate systems where sulfurization and pyritization are considered "competing," with alternate zones for each reaction. Instead, we add to the growing literature where sulfurization and pyritization can occur simultaneously (Shawar et al. 2018; Raven et al. 2019, 2021a). Further, our results imply that even in low-sulfate, high-iron environments with significant pyrite formation, lipid biomarkers may be sulfurized and potentially cross-linked into kerogens, providing a potential pathway for enhanced preservation. Future work should investigate paleo-redox environments for evidence of such biomarkers to fully realize the application to ancient and/or fully anoxic environments like early Mars or the Archaean Ocean.

Conclusions

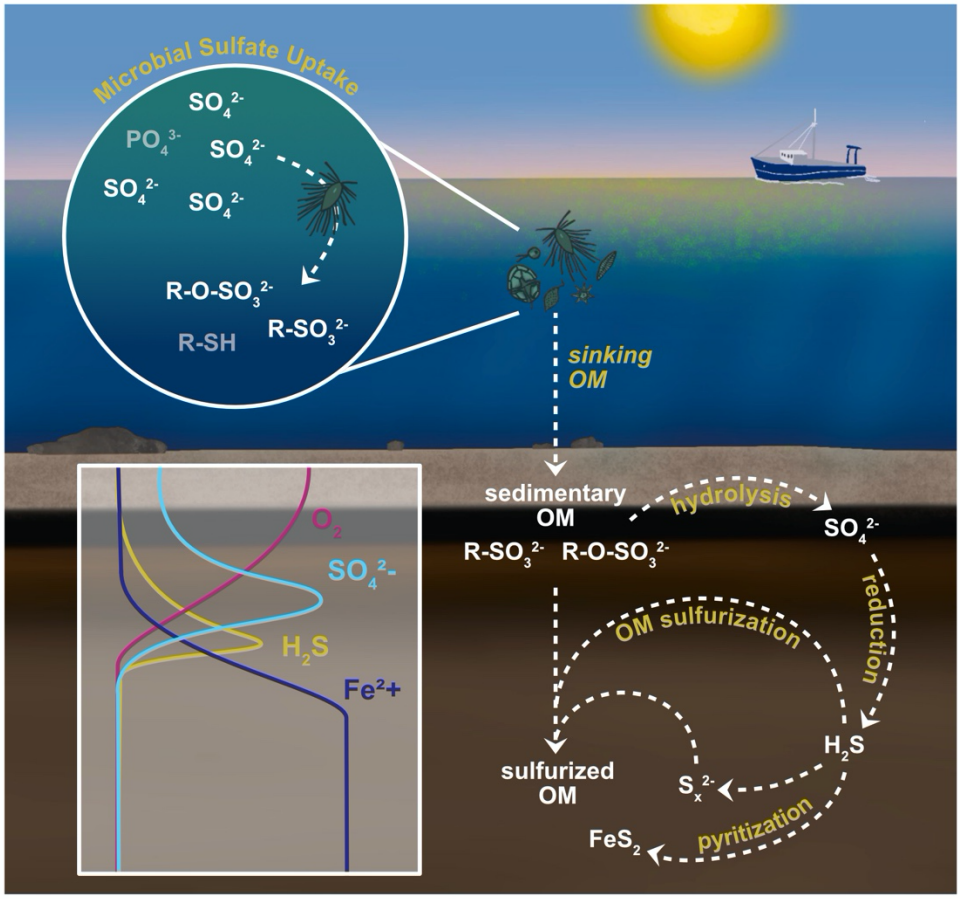

Fig 10. Conceptualization of a low-sulfate sedimentary sulfur cycle centered in organic sulfur transformations, modeled from Lake Superior's Isle Royale station.

We sought to address three outstanding questions in our microbial and geochemical investigation of Lake Superior sediments. Given previous work hypothesizing the importance of organic sulfur to sulfate reduction in this environment, we first explored the sulfur cycling potential of sedimentary microbial communities at two sites: WM and IR. WM served as a control where we did not expect active sulfate reduction due to its well-oxygenated sediments and lower organic

content. Indeed, *dsrAB* hits were unique to IR, identifying key sulfate reducers across Desulfobacterota, Nitrospirota, Acidobacteriota, and Binatota. Second, following the confirmation of this community, we explored the source of organic sulfur to sulfate reducers to determine if oxidized or reduced compounds were the more likely precursor. Using sediment incubations and sulfur speciation data, we concluded that oxidized organic sulfur in the form of lipids and polysaccharides was most likely to supply sulfate via hydrolysis. Finally, to complete our tracking from source to sink, we evaluated sulfide reactions like pyritization and sulfurization, discovering co-occurrence at the oxycline.

This case study revealed a new model of low-sulfate sulfur cycling where organic sulfur plays a central role as both a source of sulfate for microbial reduction and a sink for resulting sulfide (Fig 10). In the water column, primary producers preferentially assimilate sulfate under phosphorus starvation, producing lipids, polysaccharides, and amino acids across sulfur redox states. In the sediments, this organic matter, especially in the form of sulfonates and sulfate esters, supplies a substrate for sulfate hydrolysis via a diverse heterotrophic microbial community. Microbial sulfate reducers use this sulfate to produce sulfide in anoxic sediments, which can go on to react with iron, elemental sulfur, and organic matter to form pyrite, polysulfides, and sulfurized organic matter, respectively. Organic matter sulfurization in low sulfate may therefore preserve biomarkers with the power to constrain ancient environments and life processes. While this data is rooted in Lake Superior, we believe that these lessons regarding the relative role of organic sulfur are applicable to conceptualizing other low-sulfate systems, including the Archean Ocean.

Acknowledgements

We thank the captain, crew, and administrative team of the *R/V Blue Heron* at the University of Minnesota, Duluth (UMD). We are also grateful to students and faculty at UMD, including Jake Zunker for their help making the Lake Superior map and Dr. Melissa Maurer-Jones for assistance with the UHPLC. We also thank members of the Raven Lab at UCSB for helpful initial data discussion and manuscript revisions, especially Molly Crotteau and Lena Capece. Color-blind friendly palettes were generated from Paul Tol's online resources.

Funding

Use of the Stanford Synchrotron Radiation Lightsource, SLAC National Accelerator Laboratory (proposal 5894) is supported by the U.S. Department of Energy, Office of Science, Office of Basic Energy Sciences under contract no. DE-AC02-76SF00515. The SSRL Structural Molecular Biology Program is supported by the DOE Office of Biological and Environmental Research and by the National Institutes of Health, National Institute of General Medical Sciences (P30GM133894). The contents of this publication are solely the responsibility of the authors and do not necessarily represent the official views of NIGMS or NIH. This work was supported by the US National Science Foundation (grant number 1754061) for SK, KMS, CSS, EH and AAP. MRR acknowledges support from the UCSB Hellman Family Faculty Fellows Program. IU acknowledges funding and support from the UCSB UC 2021-2023 Leads programs.

683 **References**
684
685 Abdulla, H. A., D. J. Burdige, and T. Komada. 2020. Abiotic formation of dissolved organic
686 sulfur in anoxic sediments of Santa Barbara Basin. Organic Geochemistry **139**: 103879.
687 doi:10.1016/j.orggeochem.2019.05.009
688 Alneberg, J., B. S. Bjarnason, I. de Bruijn, and others. 2014. Binning metagenomic contigs by
689 coverage and composition. Nat Methods **11**: 1144–1146. doi:10.1038/nmeth.3103
690 Amrani, A., and Z. Aizenshtat. 2004. Reaction of polysulfide anions with α,β unsaturated
691 isoprenoid aldehydes in aquatic media: simulation of oceanic conditions. Organic
692 Geochemistry **35**: 909–921. doi:10.1016/j.orggeochem.2004.04.002
693 Amrani, A., Q. Ma, W. S. Ahmad, Z. Aizenshtat, and Y. Tang. 2008. Sulfur isotope fractionation
694 during incorporation of sulfur nucleophiles into organic compounds. Chem. Commun.
695 1356–1358. doi:10.1039/B717113G
696 Beaupré, S. R. 2015. Chapter 6 - The Carbon Isotopic Composition of Marine DOC, p. 335–368.
697 *In* D.A. Hansell and C.A. Carlson [eds.], Biogeochemistry of Marine Dissolved Organic
698 Matter (Second Edition). Academic Press.
699 Bellinger, B. J., B. A. S. Van Mooy, J. B. Cotner, and others. 2014. Physiological modifications
700 of seston in response to physicochemical gradients within Lake Superior. Limnol.
701 Oceanogr. **59**: 1011–1026. doi:10.4319/lo.2014.59.3.1011
702 Bligh, E. G., and W. J. Dyer. 1959. A Rapid Method of Total Lipid Extraction and Purification.
703 Canadian Journal of Biochemistry and Physiology **37**: 7.
704 Bollmann, A., G. S. Bullerjahn, and R. M. McKay. 2014. Abundance and Diversity of
705 Ammonia-Oxidizing Archaea and Bacteria in Sediments of Trophic End Members of the

706 Laurentian Great Lakes, Erie and Superior. PLOS ONE **9**: e97068.
707 doi:10.1371/journal.pone.0097068
708 Bottrell, S. H., and R. Raiswell. 2000. Sulphur Isotopes and Microbial Sulphur Cycling in
709 Sediments, p. 96–104. *In* R.E. Riding and S.M. Awramik [eds.], Microbial Sediments.
710 Springer.
711 Boussafir, M., F. Gelin, E. Lallier-Verges, S. Derenne, P. Bertrand, and C. Largeau. 1995.
712 Electron microscopy and pyrolysis of kerogens from the Kimmeridge Clay Formation,
713 UK: Source organisms, preservation processes, and origin of microcycles. Geochimica et
714 Cosmochimica Acta **59**: 3731–3747. doi:10.1016/0016-7037(95)00273-3
715 Boussafir, M., and E. Lallier-Verges. 1997. Accumulation of organic matter in the Kimmeridge
716 Clay formation (KCF): an update fossilisation model for marine petroleum source-rocks.
717 Marine and Petroleum Geology **14**: 75–83. doi:10.1016/S0264-8172(96)00050-5
718 Canfield, D. E. 2001. Biogeochemistry of Sulfur Isotopes. Reviews in Mineralogy and
719 Geochemistry **43**: 607–636. doi:10.2138/gsrmg.43.1.607
720 Carlton, R. G., G. S. Walker, M. J. Klug, and R. G. Wetzel. 1989. Relative Values of Oxygen,
721 Nitrate, and Sulfate to Terminal Microbial Processes in the Sediments of Lake Superior.
722 Journal of Great Lakes Research **15**: 133–140. doi:10.1016/S0380-1330(89)71467-2
723 Chaumeil, P.-A., A. J. Mussig, P. Hugenholtz, and D. H. Parks. 2020. GTDB-Tk: a toolkit to
724 classify genomes with the Genome Taxonomy Database. Bioinformatics **36**: 1925–1927.
725 doi:10.1093/bioinformatics/btz848
726 Chen, L.-X., K. Anantharaman, A. Shaiber, A. M. Eren, and J. F. Banfield. 2020. Accurate and
727 complete genomes from metagenomes. Genome Res **30**: 315–333.
728 doi:10.1101/gr.258640.119

729 Chen, S., Y. Zhou, Y. Chen, and J. Gu. 2018. fastp: an ultra-fast all-in-one FASTQ preprocessor.
730 Bioinformatics **34**: i884–i890. doi:10.1093/bioinformatics/bty560
731 Crowe, S. A., G. Paris, S. Katsev, and others. 2014. Sulfate was a trace constituent of Archean
732 seawater. Science **346**: 735–739. doi:10.1126/science.1258966
733 Crowe, S. A., A. H. Treusch, M. Forth, J. Li, C. Magen, D. E. Canfield, B. Thamdrup, and S.
734 Katsev. 2017. Novel anammox bacteria and nitrogen loss from Lake Superior. Sci Rep **7**:
735 13757. doi:10.1038/s41598-017-12270-1
736 Davis, K. E. R., P. Sangwan, and P. H. Janssen. 2011. Acidobacteria, Rubrobacteridae and
737 Chloroflexi are abundant among very slow-growing and mini-colony-forming soil
738 bacteria. Environmental Microbiology **13**: 798–805. doi:10.1111/j.1462-
739 2920.2010.02384.x
740 Davison, W., J. P. Lishman, and J. Hilton. 1985. Formation of pyrite in freshwater sediments:
741 Implications for C/S ratios. Geochimica et Cosmochimica Acta **49**: 1615–1620.
742 doi:10.1016/0016-7037(85)90266-2
743 Dittmar, T., B. Koch, N. Hertkorn, and G. Kattner. 2008. A simple and efficient method for the
744 solid-phase extraction of dissolved organic matter (SPE-DOM) from seawater.
745 Limnology and Oceanography: Methods **6**: 230–235.
746 doi:https://doi.org/10.4319/lom.2008.6.230
747 Dittrich, M., L. Moreau, J. Gordon, and others. 2015. Geomicrobiology of Iron Layers in the
748 Sediment of Lake Superior. Aquat Geochem **21**: 123–140. doi:10.1007/s10498-015-
749 9258-y

van Dongen, B., S. Schouten, M. Baas, J. Geenevasen, and J. Sinninghe-Damste. 2003. An experimental study of the low-temperature sulfurization of carbohydrates. Organic Geochemistry **34**: 1129–1144. doi:10.1016/S0146-6380(03)00060-3

Durham, B. P., S. Sharma, H. Luo, and others. 2015. Cryptic carbon and sulfur cycling between surface ocean plankton. Proceedings of the National Academy of Sciences **112**: 453–457. doi:10.1073/pnas.1413137112

Elul, M., M. Rubin-Blum, Z. Ronen, I. Bar-Or, W. Eckert, and O. Sivan. 2021. Metagenomic insights into the metabolism of microbial communities that mediate iron and methane cycling in Lake Kinneret iron-rich methanic sediments. Biogeosciences **18**: 2091–2106. doi:10.5194/bg-18-2091-2021

Fahnenstiel, G. L., L. Sicko-Goad, D. Scavia, and E. F. Stoermer. 1986. Importance of Picoplankton in Lake Superior. Can. J. Fish. Aquat. Sci. **43**: 235–240. doi:10.1139/f86-028

Fakhraee, M., and S. Katsev. 2019. Organic sulfur was integral to the Archean sulfur cycle. Nat Commun **10**: 4556. doi:10.1038/s41467-019-12396-y

Fakhraee, M., J. Li, and S. Katsev. 2017. Significant role of organic sulfur in supporting sedimentary sulfate reduction in low-sulfate environments. Geochimica et Cosmochimica Acta **213**: 502–516. doi:10.1016/j.gca.2017.07.021

Ferdelman, T. G., T. M. Church, and G. W. Luther. 1991. Sulfur enrichment of humic substances in a Delaware salt marsh sediment core. Geochimica et Cosmochimica Acta **55**: 979–988. doi:10.1016/0016-7037(91)90156-Y

Finster, K. 2008. Microbiological disproportionation of inorganic sulfur compounds. Journal of Sulfur Chemistry **29**: 281–292. doi:10.1080/17415990802105770

773 Fitzgerald, J. W. 1976. Sulfate ester formation and hydrolysis: a potentially important yet often
774 ignored aspect of the sulfur cycle of aerobic soils. Bacteriol Rev **40**: 698–721.
775 Flieder, M., J. Buongiorno, C. W. Herbold, B. Hausmann, T. Rattei, K. G. Lloyd, A. Loy, and K.
776 Wasmund. 2021. Novel taxa of Acidobacteriota implicated in seafloor sulfur cycling.
777 ISME J **15**: 3159–3180. doi:10.1038/s41396-021-00992-0
778 Francois, R. 1987. A study of sulphur enrichment in the humic fraction of marine sediments
779 during early diagenesis. Geochimica et Cosmochimica Acta **51**: 17–27.
780 doi:10.1016/0016-7037(87)90003-2
781 Gomes, M. L., J. M. Klatt, G. J. Dick, and others. 2022. Sedimentary pyrite sulfur isotope
782 compositions preserve signatures of the surface microbial mat environment in sediments
783 underlying low-oxygen cyanobacterial mats. Geobiology **20**: 60–78.
784 doi:10.1111/gbi.12466
785 Hyatt, D., G.-L. Chen, P. F. LoCascio, M. L. Land, F. W. Larimer, and L. J. Hauser. 2010.
786 Prodigal: prokaryotic gene recognition and translation initiation site identification. BMC
787 Bioinformatics **11**: 119. doi:10.1186/1471-2105-11-119
788 Ivanikova, N. V., L. C. Popels, R. M. L. McKay, and G. S. Bullerjahn. 2007. Lake Superior
789 Supports Novel Clusters of Cyanobacterial Picoplankton. Applied and Environmental
790 Microbiology **73**: 4055–4065. doi:10.1128/AEM.00214-07
791 Ivanova, A. A., A. D. Zhelezova, T. I. Chernov, and S. N. Dedysh. 2020. Linking ecology and
792 systematics of acidobacteria: Distinct habitat preferences of the Acidobacteriia and
793 Blastocatellia in tundra soils. PLOS ONE **15**: e0230157.
794 doi:10.1371/journal.pone.0230157

795 Jiang, M., Y. Sheng, Q. Liu, W. Wang, and X. Liu. 2021. Conversion mechanisms between
796 organic sulfur and inorganic sulfur in surface sediments in coastal rivers. Science of The
797 Total Environment **752**: 141829. doi:10.1016/j.scitotenv.2020.141829
798 Johnson, T. C., J. E. Evans, and S. J. Eisenreich. 1982. Total organic carbon in Lake Superior
799 sediments: Comparisons with hemipelagic and pelagic marine environments1. Limnology
800 and Oceanography **27**: 481–491. doi:10.4319/lo.1982.27.3.0481
801 Jorgensen, B. B. 1979. A theoretical model of the stable sulfur isotope distribution in marine
802 sediments. Geochimica et Cosmochimica Acta **43**: 363–374. doi:10.1016/0016-
803 7037(79)90201-1
804 Jørgensen, B. B., A. J. Findlay, and A. Pellerin. 2019. The Biogeochemical Sulfur Cycle of
805 Marine Sediments. Front. Microbiol. **10**. doi:10.3389/fmicb.2019.00849
806 Kang, D. D., J. Froula, R. Egan, and Z. Wang. 2015. MetaBAT, an efficient tool for accurately
807 reconstructing single genomes from complex microbial communities. PeerJ **3**: e1165.
808 doi:10.7717/peerj.1165
809 Kang, D. D., F. Li, E. Kirton, A. Thomas, R. Egan, H. An, and Z. Wang. 2019. MetaBAT 2: an
810 adaptive binning algorithm for robust and efficient genome reconstruction from
811 metagenome assemblies. PeerJ **7**: e7359. doi:10.7717/peerj.7359
812 Kemp, A. L. W., C. I. Dell, and N. S. Harper. 1978. Sedimentation Rates and a Sediment Budget
813 for Lake Superior. Journal of Great Lakes Research **4**: 276–287. doi:10.1016/S0380-
814 1330(78)72198-2
815 King, G. M., and M. J. Klug. 1982. Comparative aspects of sulfur mineralization in sediments of
816 a eutrophic lake basin. Appl Environ Microbiol **43**: 1406–1412.
817 doi:10.1128/aem.43.6.1406-1412.1982

Kohnen, M. E. L., J. S. S. Damsté, H. L. ten Haven, and J. W. de Leeuw. 1989. Early incorporation of polysulphides in sedimentary organic matter. Nature **341**: 640–641. doi:10.1038/341640a0

Kok, M. D., W. I. C. Rijpstra, L. Robertson, J. K. Volkman, and J. S. Sinninghe Damstéé. 2000. Early steroid sulfurisation in surface sediments of a permanently stratified lake (Ace Lake, Antarctica). Geochimica et Cosmochimica Acta **64**: 1425–1436. doi:10.1016/S0016-7037(99)00430-5

Kokkonen, P., and K. Tolonen. 1987. Analysis of organic and inorganic sulfur constituents and 34S-isotopes in dated sediments of Forest Lakes in southern Finland. Water Air Soil Pollut **35**: 157–170. doi:10.1007/BF00183851

Ksionzek, K. B., O. J. Lechtenfeld, S. L. McCallister, P. Schmitt-Kopplin, J. K. Geuer, W. Geibert, and B. P. Koch. 2016. Dissolved organic sulfur in the ocean: Biogeochemistry of a petagram inventory. Science **354**: 456–459. doi:10.1126/science.aaf7796

de Leeuw, J., and J. Sinninghe-Damste. 1990. Organic Sulfur Compounds and Other Biomarkers as Indicators of Palaeosalinity. Acs Symposium Series - ACS SYMP SER **429**: 417–443. doi:10.1021/bk-1990-0429.ch024

Li, J. 2014. Sediment diagenesis in large lakes Superior and Malawi, geochemical cycles and budgets and comparisons to marine sediments.

Li, J., S. A. Crowe, D. Miklesh, M. Kistner, D. E. Canfield, and S. Katsev. 2012. Carbon mineralization and oxygen dynamics in sediments with deep oxygen penetration, Lake Superior. Limnology and Oceanography **57**: 1634–1650. doi:10.4319/lo.2012.57.6.1634

839 Li, J., and S. Katsev. 2014. Nitrogen cycling in deeply oxygenated sediments: Results in Lake
840 Superior and implications for marine sediments. Limnology and Oceanography **59**: 465–
841 481. doi:10.4319/lo.2014.59.2.0465
842 Li, J., Y. Zhang, and S. Katsev. 2018. Phosphorus recycling in deeply oxygenated sediments in
843 Lake Superior controlled by organic matter mineralization. Limnology and
844 Oceanography **63**: 1372–1385. doi:10.1002/lno.10778
845 Lie, T. J., J. R. Leadbetter, and E. R. Leadbetter. 1998. Metabolism of sulfonic acids and other
846 organosulfur compounds by sulfate-reducing bacteria. Geomicrobiology Journal **15**: 135–
847 149. doi:10.1080/01490459809378070
848 Ma, J., K. L. French, X. Cui, D. A. Bryant, and R. E. Summons. 2021. Carotenoid biomarkers in
849 Namibian shelf sediments: Anoxygenic photosynthesis during sulfide eruptions in the
850 Benguela Upwelling System. Proceedings of the National Academy of Sciences **118**:
851 e2106040118. doi:10.1073/pnas.2106040118
852 Mateos, K., G. Chappell, E. Stüeken, and R. Anderson. 2022. The evolution and spread of sulfur-
853 cycling enzymes reflect volcanic sulfur sources and the redox state of the early Earth.
854 2022.08.05.502933. doi:10.1101/2022.08.05.502933
855 Minor, E. C., C. J. Tennant, and E. T. Brown. 2019. A Seasonal to Interannual View of Inorganic
856 and Organic Carbon and pH in Western Lake Superior. Journal of Geophysical Research:
857 Biogeosciences **124**: 405–419. doi:10.1029/2018JG004664
858 Moran, M. A., and B. P. Durham. 2019. Sulfur metabolites in the pelagic ocean. Nature Reviews
859 Microbiology **17**: 665–678. doi:10.1038/s41579-019-0250-1
860 Murphy, C. L., A. Sheremet, P. F. Dunfield, J. R. Spear, R. Stepanauskas, T. Woyke, M. S.
861 Elshahed, and N. H. Youssef. Genomic Analysis of the Yet-Uncultured Binatota Reveals

Broad Methylotrophic, Alkane-Degradation, and Pigment Production Capacities. mBio **12**: e00985-21. doi:10.1128/mBio.00985-21

Nriagu, J. O., and Y. K. Soon. 1985. Distribution and isotopic composition of sulfur in lake sediments of northern Ontario. Geochimica et Cosmochimica Acta **49**: 823–834. doi:10.1016/0016-7037(85)90175-9

Nurk, S., D. Meleshko, A. Korobeynikov, and P. A. Pevzner. 2017. metaSPAdes: a new versatile metagenomic assembler. Genome Res **27**: 824–834. doi:10.1101/gr.213959.116

O'Beirne, M. D., J. P. Werne, R. E. Hecky, T. C. Johnson, S. Katsev, and E. D. Reavie. 2017. Anthropogenic climate change has altered primary productivity in Lake Superior. Nat Commun **8**: 15713. doi:10.1038/ncomms15713

Olm, M. R., C. T. Brown, B. Brooks, and J. F. Banfield. 2017. dRep: a tool for fast and accurate genomic comparisons that enables improved genome recovery from metagenomes through de-replication. ISME J **11**: 2864–2868. doi:10.1038/ismej.2017.126

Orellana, L. H., T. B. Francis, M. Ferraro, J.-H. Hehemann, B. M. Fuchs, and R. I. Amann. 2022. Verrucomicrobiota are specialist consumers of sulfated methyl pentoses during diatom blooms. ISME J **16**: 630–641. doi:10.1038/s41396-021-01105-7

Palermo, C., and M. Dittrich. 2016. Evidence for the biogenic origin of manganese-enriched layers in Lake Superior sediments. Environmental Microbiology Reports **8**: 179–186. doi:10.1111/1758-2229.12364

Parks, D. H., M. Imelfort, C. T. Skennerton, P. Hugenholtz, and G. W. Tyson. 2015. CheckM: assessing the quality of microbial genomes recovered from isolates, single cells, and metagenomes. Genome Res **25**: 1043–1055. doi:10.1101/gr.186072.114

884 Phillips, A. A., M. E. White, M. Seidel, and others. 2022. Novel sulfur isotope analyses constrain
885 sulfurized porewater fluxes as a minor component of marine dissolved organic matter.
886 Proceedings of the National Academy of Sciences **119**: e2209152119.
887 doi:10.1073/pnas.2209152119
888 Phillips, A. A., F. Wu, and A. L. Sessions. 2021. Sulfur isotope analysis of cysteine and
889 methionine via preparatory liquid chromatography and elemental analyzer isotope ratio
890 mass spectrometry. Rapid Communications in Mass Spectrometry **35**: e9007.
891 doi:https://doi.org/10.1002/rcm.9007
892 Prahl, F. G., L. A. Pinto, and M. A. Sparrow. 1996. Phytane from chemolytic analysis of modern
893 marine sediments: A product of desulfurization or not? Geochimica et Cosmochimica
894 Acta **60**: 1065–1073. doi:10.1016/0016-7037(95)00450-5
895 Raven, M. R., D. A. Fike, A. S. Bradley, M. L. Gomes, J. D. Owens, and S. A. Webb. 2019.
896 Paired organic matter and pyrite δ34S records reveal mechanisms of carbon, sulfur, and
897 iron cycle disruption during Ocean Anoxic Event 2. Earth and Planetary Science Letters
898 **512**: 27–38. doi:10.1016/j.epsl.2019.01.048
899 Raven, M. R., D. A. Fike, M. L. Gomes, S. M. Webb, A. S. Bradley, and H.-L. O. McClelland.
900 2018. Organic carbon burial during OAE2 driven by changes in the locus of organic
901 matter sulfurization. Nature Communications **9**: 3409. doi:10.1038/s41467-018-05943-6
902 Raven, M. R., R. G. Keil, and S. M. Webb. 2020. Microbial sulfate reduction and organic sulfur
903 formation in sinking marine particles. Science. doi:10.1126/science.abc6035
904 Raven, M. R., R. G. Keil, and S. M. Webb. 2021a. Rapid, Concurrent Formation of Organic
905 Sulfur and Iron Sulfides During Experimental Sulfurization of Sinking Marine Particles.
906 Global Biogeochemical Cycles **35**: e2021GB007062. doi:10.1029/2021GB007062

907 Raven, M. R., R. G. Keil, and S. M. Webb. 2021b. Microbial sulfate reduction and organic sulfur
908 formation in sinking marine particles. Science **371**: 178–181.
909 doi:10.1126/science.abc6035
910 Reed, A. J., and R. E. Hicks. 2011. Microbial ecology of Lake Superior *Bacteria* and *Archaea* :
911 An overview. Aquatic Ecosystem Health & Management **14**: 386–395.
912 doi:10.1080/14634988.2011.630282
913 Rickard, D., and G. W. Luther. 2007. Chemistry of Iron Sulfides. Chem. Rev. **107**: 514–562.
914 doi:10.1021/cr0503658
915 Roy, A. B. 1971. 1 The Hydrolysis of Sulfate Esters, p. 1–19. *In* P.D. Boyer [ed.], The Enzymes.
916 Academic Press.
917 Saito, M. A., D. M. Sigman, and F. M. M. Morel. 2003. The bioinorganic chemistry of the
918 ancient ocean: the co-evolution of cyanobacterial metal requirements and biogeochemical
919 cycles at the Archean–Proterozoic boundary? Inorganica Chimica Acta **356**: 308–318.
920 doi:10.1016/S0020-1693(03)00442-0
921 Shaffer, M., M. A. Borton, B. B. McGivern, and others. 2020. DRAM for distilling microbial
922 metabolism to automate the curation of microbiome function. Nucleic Acids Research **48**:
923 8883–8900. doi:10.1093/nar/gkaa621
924 Shawar, L., I. Halevy, W. Said-Ahmad, S. Feinstein, V. Boyko, A. Kamyshny, and A. Amrani.
925 2018. Dynamics of pyrite formation and organic matter sulfurization in organic-rich
926 carbonate sediments. Geochimica et Cosmochimica Acta **241**: 219–239.
927 doi:10.1016/j.gca.2018.08.048

928 Sheik, C. S., K. E. Natwora, E. E. Alexson, and others. 2022. Dolichospermum blooms in Lake
929 Superior: DNA-based approach provides insight to the past, present and future of blooms.
930 Journal of Great Lakes Research **48**: 1191–1205. doi:10.1016/j.jglr.2022.08.002
931 Shivlata, L., and T. Satyanarayana. 2015. Thermophilic and alkaliphilic Actinobacteria: biology
932 and potential applications. Front Microbiol **6**: 1014. doi:10.3389/fmicb.2015.01014
933 Sieber, C. M. K., A. J. Probst, A. Sharrar, B. C. Thomas, M. Hess, S. G. Tringe, and J. F.
934 Banfield. 2018. Recovery of genomes from metagenomes via a dereplication, aggregation
935 and scoring strategy. Nat Microbiol **3**: 836–843. doi:10.1038/s41564-018-0171-1
936 Silverman, S. N., A. A. Phillips, G. M. Weiss, E. B. Wilkes, J. M. Eiler, and A. L. Sessions.
937 2022. Practical considerations for amino acid isotope analysis. Organic Geochemistry
938 **164**: 104345. doi:10.1016/j.orggeochem.2021.104345
939 Sinninghe Damsté, J. S., M. D. Kok, J. Köster, and S. Schouten. 1998. Sulfurized carbohydrates:
940 an important sedimentary sink for organic carbon? Earth and Planetary Science Letters
941 **164**: 7–13. doi:10.1016/S0012-821X(98)00234-9
942 Small, G. E., J. C. Finlay, R. M. L. McKay, M. J. Rozmarynowycz, S. Brovold, G. S. Bullerjahn,
943 K. Spokas, and R. W. Sterner. 2016. Large differences in potential denitrification and
944 sediment microbial communities across the Laurentian great lakes. Biogeochemistry **128**:
945 353–368. doi:10.1007/s10533-016-0212-x
946 Smith, D. A., A. L. Sessions, K. S. Dawson, N. Dalleska, and V. J. Orphan. 2017. Rapid
947 quantification and isotopic analysis of dissolved sulfur species: Quantification and
948 isotopic analysis of dissolved sulfur species. Rapid Commun. Mass Spectrom. **31**: 791–
949 803. doi:10.1002/rcm.7846

Sterner, R. 2011. C:N:P stoichiometry in Lake Superior: freshwater sea as end member. IW **1**: 29–46. doi:10.5268/IW-1.1.365

Sterner, R. W. 2010. In situ-measured primary production in Lake Superior. Journal of Great Lakes Research **36**: 139–149. doi:10.1016/j.jglr.2009.12.007

Sterner, R. W., E. Anagnostou, S. Brovold, G. S. Bullerjahn, J. C. Finlay, S. Kumar, R. M. L. McKay, and R. M. Sherrell. 2007. Increasing stoichiometric imbalance in North America's largest lake: Nitrification in Lake Superior. Geophysical Research Letters **34**. doi:10.1029/2006GL028861

Suominen, S., D. M. van Vliet, I. Sánchez-Andrea, M. T. J. van der Meer, J. S. Sinninghe Damsté, and L. Villanueva. 2021. Organic Matter Type Defines the Composition of Active Microbial Communities Originating From Anoxic Baltic Sea Sediments. Frontiers in Microbiology **12**.

Umezawa, K., H. Kojima, Y. Kato, and M. Fukui. 2021. Dissulfurispira thermophila gen. nov., sp. nov., a thermophilic chemolithoautotroph growing by sulfur disproportionation, and proposal of novel taxa in the phylum Nitrospirota to reclassify the genus Thermodesulfovibrio. Systematic and Applied Microbiology **44**: 126184. doi:10.1016/j.syapm.2021.126184

Urban, N. R., K. Ernst, and S. Bernasconi. 1999. Addition of sulfur to organic matter during early diagenesis of lake sediments. Geochimica et Cosmochimica Acta **63**: 837–853. doi:10.1016/S0016-7037(98)00306-8

Vairavamurthy, A. 1998. Using X-ray absorption to probe sulfur oxidation states in complex molecules. Spectrochimica Acta Part A: Molecular and Biomolecular Spectroscopy **54**: 2009–2017. doi:10.1016/S1386-1425(98)00153-X

973 Van Kaam-Peters, H. M. E., S. Schouten, J. Köster, and J. S. Sinninghe Damstè. 1998. Controls
974 on the molecular and carbon isotopic composition of organic matter deposited in a
975 Kimmeridgian euxinic shelf sea: evidence for preservation of carbohydrates through
976 sulfurisation. Geochimica et Cosmochimica Acta **62**: 3259–3283. doi:10.1016/S0016-
977 7037(98)00231-2
978 Van Mooy, B. A. S., H. F. Fredricks, B. E. Pedler, and others. 2009. Phytoplankton in the ocean
979 use non-phosphorus lipids in response to phosphorus scarcity. Nature **458**: 69–72.
980 doi:10.1038/nature07659
981 van Vliet, D. M., F. A. B. von Meijenfeldt, B. E. Dutilh, L. Villanueva, J. S. Sinninghe Damsté,
982 A. J. M. Stams, and I. Sánchez-Andrea. 2021. The bacterial sulfur cycle in expanding
983 dysoxic and euxinic marine waters. Environmental Microbiology **23**: 2834–2857.
984 doi:10.1111/1462-2920.15265
985 Webb, S. SIXpack: a graphical user interface for XAS analysis using IFEFFIT - IOPscience.
986 Williams, T. J., M. A. Allen, J. F. Berengut, and R. Cavicchioli. 2021. Shedding Light on
987 Microbial “Dark Matter”: Insights Into Novel Cloacimonadota and Omnitrophota From
988 an Antarctic Lake. Frontiers in Microbiology **12**.
989 Woodcroft, B. J. 2023. CoverM.
990 Wu, Y.-W., B. A. Simmons, and S. W. Singer. 2016. MaxBin 2.0: an automated binning
991 algorithm to recover genomes from multiple metagenomic datasets. Bioinformatics **32**:
992 605–607. doi:10.1093/bioinformatics/btv638
993 Xing, M., Y. Wei, Y. Zhou, and others. 2019. Radical-mediated C-S bond cleavage in C2
994 sulfonate degradation by anaerobic bacteria. Nat Commun **10**: 1609. doi:10.1038/s41467-
995 019-09618-8

Zhu, G., T. Li, T. Huang, K. Zhao, W. Tang, R. Wang, X. Lang, and B. Shen. 2021. Quantifying the Seawater Sulfate Concentration in the Cambrian Ocean. Frontiers in Earth Science **9**.

Zigah, P. K., E. C. Minor, J. P. Werne, and S. L. McCallister. 2011. Radiocarbon and stable carbon isotopic insights into provenance and cycling of carbon in Lake Superior. Limnology and Oceanography **56**: 867–886. doi:10.4319/lo.2011.56.3.0867